How Land Surface Characteristics Influence the Development of Flash Drought through the Drivers of Soil Moisture and Vapor Pressure Deficit

LAUREN E. L. LOWMAN,[a] JORDAN I. CHRISTIAN,[b] AND ERIC D. HUNT[c]

[a] *Department of Engineering, Wake Forest University, Winston-Salem, North Carolina*
[b] *School of Meteorology, University of Oklahoma, Norman, Oklahoma*
[c] *School of Natural Resources, University of Nebraska–Lincoln, Lincoln, Nebraska*

(Manuscript received 12 September 2022, in final form 1 May 2023, accepted 7 June 2023)

ABSTRACT: As global mean temperature rises, extreme drought events are expected to increasingly affect regions of the United States that are crucial for agriculture, forestry, and natural ecology. A pressing need is to understand and anticipate the conditions under which extreme drought causes catastrophic failure to vegetation in these areas. To better predict drought impacts on ecosystems, we first must understand how specific drivers, namely, atmospheric aridity and soil water stress, affect land surface processes during the evolution of flash drought events. In this study, we evaluated when vapor pressure deficit (VPD) and soil moisture thresholds corresponding to photosynthetic shutdown were crossed during flash drought events across different climate zones and land surface characteristics in the United States. First, the Dynamic Canopy Biophysical Properties (DCBP) model was used to estimate the thresholds that define reduced photosynthesis by assimilating vegetation phenology data from the Moderate Resolution Imaging Spectroradiometer (MODIS) to a predictive phenology model. Next, we characterized and quantified flash drought onset, intensity, and duration using the standardized evaporative stress ratio (SESR) and NLDAS-2 reanalysis. Once periods of flash drought were identified, we investigated how VPD and soil moisture coevolved across regions and plant functional types. Results demonstrate that croplands and grasslands tend to be more sensitive to soil water limitations than trees across different regions of the United States. We found that whether VPD or soil moisture was the primary driver of plant water stress during drought was largely region specific. The results of this work will help to inform land managers of early warning signals relevant for specific ecosystems under threat of flash drought events.

KEYWORDS: Ecosystem effects; Humidity; Soil moisture; Stress; Water budget/balance

1. Introduction

Drought is a recurring feature of the natural climate system that is often identified as falling into one or more of five categories: meteorological, agricultural, hydrological, socioeconomic, and ecological (Wilhite and Glantz 1985; Crausbay et al. 2017). When drought persists for years over a large area, such as the western United States in the early twenty-first century, the term "megadrought" has been adopted (Williams et al. 2020). At the other end of the temporal spectrum, droughts can develop rapidly on subseasonal time scales, also known as flash drought (Svoboda et al. 2002; Otkin et al. 2013, 2016, 2019; Hunt et al. 2014; Ford et al. 2015; McEvoy et al. 2016; Lisonbee et al. 2021; Pendergrass et al. 2020). In recent years, flash droughts have been among the costliest natural disasters experienced in the United States as a result of damages to agricultural lands and forests (e.g., Smith 2020; Otkin et al. 2016). The rapid onset of flash drought makes it difficult to assess whether drying conditions in the soil or atmosphere are driving the negative outcomes observed on the land surface.

The term flash drought has been proposed for droughts that develop more rapidly than conventional drought. Flash droughts are defined by a rapid onset and intensification of dry conditions caused by a lack of precipitation in combination with above average air temperatures, wind speeds, solar radiation, and lower humidity (Otkin et al. 2018). Flash droughts are more likely to occur in regions of transition from humid to semiarid climate regimes and in regions where the landscape is dominated by row crop agriculture (Christian et al. 2019b, 2021). Further, flash drought can lead to compound events (e.g., heat wave) and cascading impacts (e.g., food security impacts; Hunt et al. 2021).

Over the past decade, several regions of the United States have experienced notable flash drought events. Examples include the spring and summer of 2011 across the south-central United States (Luo and Zhang 2012), the summer of 2012 across the central United States (Rippey 2015; Basara et al. 2019), the fall of 2016 across the Southeast (Williams et al. 2017), and the summer of 2017 across the northern Great Plains (He et al. 2019). Flash droughts have been diagnosed through standardized anomalies of near-surface and subsurface variables. These include soil moisture (Hunt et al. 2014; Ford and Labosier 2017; Osman et al. 2021), temperature and precipitation (Mo and Lettenmaier 2015), and evaporative stress (Otkin et al. 2013, 2014; Christian et al. 2019b).

Flash drought can also be monitored in near–real time with indices sensitive to rapid changes in hydrometeorological

Denotes content that is immediately available upon publication as open access.

Supplemental information related to this paper is available at the Journals Online website: https://doi.org/10.1175/JHM-D-22-0158.s1.

Corresponding author: Lauren E. L. Lowman, lowmanle@wfu.edu

DOI: 10.1175/JHM-D-22-0158.1

conditions. Examples include, but are not limited to, a soil moisture index (SMI; Hunt et al. 2009), evaporative stress index (ESI; Anderson et al. 2007a,b), standardized precipitation evapotranspiration index (SPEI; Vicente-Serrano et al. 2010), rapid change index (RCI; Otkin et al. 2014), a flash drought intensity index (Otkin et al. 2021), and land surface water index (Christian et al. 2022). In addition, the standardized evaporative stress ratio (SESR) was developed to diagnose flash drought in the United States (Christian et al. 2019b) and around the globe (Christian et al. 2021). SESR is advantageous for flash drought analysis as it has the potential to diagnose both the drivers and impact of flash drought by accounting for evapotranspiration (ET) and potential evapotranspiration (PET) at a particular location and given time. As such, SESR is sensitive to areas where ET reductions are occurring from water stress and where the atmospheric demand is greater than normal, due to increased temperature and vapor pressure deficit. While SESR is based on anomalies in evapotranspiration, the metric itself has been demonstrated to capture both meteorological and agricultural drought (i.e., daily to subseasonal time scales; Edris et al. 2023), and changes in vegetation water status as characterized through the land surface water index (LSWI; Christian et al. 2022).

Water stress in the atmosphere and soils can severely limit vegetation functioning, and can result in worsening drought conditions. High atmospheric aridity, often measured as vapor pressure deficit (VPD), and low soil moisture lead plants to reduce or completely stop photosynthesis to minimize water losses through pores in the leaves (e.g., Oren et al. 1999). Compound drought, where both low soil moisture and high atmospheric aridity occur, are enhanced by land–atmosphere feedbacks controlled by plant gas exchange (Zhou et al. 2019). The key mechanism that describes the ability for plants to regulate water losses under stress conditions is referred to as conductance (e.g., Medrano et al. 2002). Separating the ecosystem impacts that result from elevated VPD and low soil moisture observed during drought is challenging as the two are strongly coupled (Fu et al. 2022; Rigden et al. 2020; Kimm et al. 2020; Liu et al. 2020; Novick et al. 2016; Sulman et al. 2016). Recently, conditional probabilities for changes in plant productivity linked to atmospheric dryness or soil water depletion have been constructed by binning events with high and low ranges of VPD and soil water content (Liu et al. 2020; Fu et al. 2022). Using this approach, elevated values of VPD were demonstrated to negatively impact plant productivity along a range of soil moisture values from both eddy-covariance data and Earth system models (Fu et al. 2022). Sulman et al. (2016) and Novick et al. (2016) evaluated changes in photosynthesis and transpiration associated with high VPD and low soil moisture and found that fluctuations in VPD led to reductions in fluxes of water and carbon controlled by plant activity. In croplands located in the central United States, VPD was found to exert a stronger control on variability in canopy conductance using observations of VPD and soil moisture data from individual AmeriFlux sites (Kimm et al. 2020). Conversely, Rigden et al. (2020) found that predictions of maize crop yields conditioned on VPD, rather than soil moisture, would lead to inaccurate estimates of damage.

In addition to atmospheric conditions that can negatively impact vegetation function, different land cover types may also promote or moderate flash drought development. For example, the central United States is a regional hotspot for land–atmosphere coupling (Koster et al. 2004; Dirmeyer 2011), and positive feedbacks between dry soils, limited evapotranspiration, and increased evaporative demand may enhance the rate of intensification toward drought (Gerken et al. 2018; Basara et al. 2019; Chen et al. 2021). Specific land cover types may also limit flash drought development. During a lack of precipitation and above average temperatures, greenness and productivity of forests do not decline as much as grassland and agricultural areas due to the deeper rooting depths of forests (Cui et al. 2019). As a result, sustained evapotranspiration may limit excessive evaporative stress and flash drought development over vegetation in forest-dominated areas, compared to agricultural locations that more quickly deplete near-surface and root-zone soil moisture (Christian et al. 2020). However, the role land cover types play in flash drought development has not been extensively investigated, and remains a critical topic to be addressed.

In this manuscript, we investigated the land surface impact of flash drought via soil moisture and vapor pressure deficit during known flash drought events in the contiguous United States (CONUS) that occurred from 2010 to 2020. Specifically, we evaluated how flash drought development related to worsening conditions defined by a coincidental increase in VPD and a decrease in soil moisture. This is done by using SESR as an independent metric to determine flash drought onset and duration. Then, we evaluated how the stress conditions of VPD and soil moisture evolved during the defined flash drought period. We focused on the sensitivity of vegetation to anomalies in VPD and soil moisture during flash drought, because these events create rapidly deteriorating conditions for vegetation that alter their growth and photosynthetic activity at short time scales (i.e., daily to subseasonal). Special attention is given to how flash drought development differs across different land cover types within the same climate region. The main research question we seek to answer is, "How does the land surface response to flash drought differ by land cover characteristics and what drives the observed differences?"

2. Methods

The goal of this study was to characterize flash drought events by the driving environmental factors that led to stunted vegetation growth and/or complete shutdown of photosynthetic activity. First, SESR is used to independently determine the spatiotemporal bounds of flash drought. Second, we use reanalysis data along with a predictive phenology model to determine the parameters of VPD and soil moisture that bracket the range of suboptimal vegetation function (i.e., between uninhibited photosynthesis and complete stomatal closure). Finally, we evaluate whether or not VPD or soil moisture conditions during the flash drought event surpassed maximum VPD or minimum soil moisture where stomata are closed and photosynthetic function shuts down. This indicates that conditions during

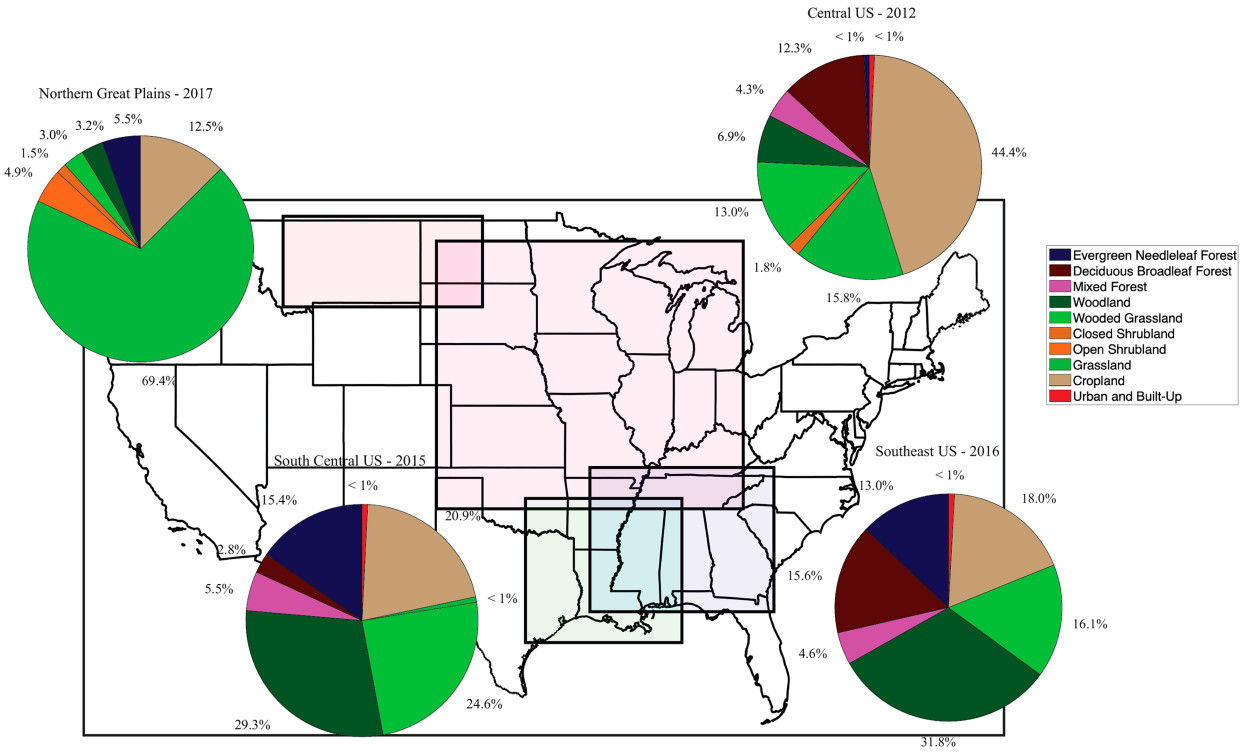

FIG. 1. Domains of the study regions, including the central United States during 2012 (purple), the south-central United States in 2015 (green), the Southeast in 2016 (blue), and the northern Great Plains in 2017 (pink). Proportions of land cover types that make up each region are summarized as pie charts.

the flash drought worsened to the point that plants could no longer be productive. The overall method developed for this study consists of the following steps:

1) Flash drought events were identified and characterized by their onset and duration using SESR.
2) Thresholds for suboptimal vegetation function were determined based on land cover type, soil texture, and climate using a predictive phenology model.
3) Exceedance probabilities of crossing VPD and soil water potential thresholds are determined for each region before, during, and after the flash drought event.

The following subsections describe the data and procedures used in this study for identifying flash drought events and characterizing thresholds for suboptimal vegetation function.

a. Study regions

To evaluate the influence of regional climate and vegetation type on the sensitivity of land cover response to deteriorating soil moisture and VPD conditions, study regions were selected using a set of criteria. In this study, specific flash drought events and their corresponding spatial extent were selected as study regions using the following criteria: 1) the flash drought event was unambiguous and can be corroborated within the existing literature, 2) selected events differ in terms of climate and/or geographic region within CONUS, and 3) study areas are comprised of different proportions of land cover types. We additionally sought out case studies in which the duration of the rapid intensification characteristic of flash droughts varied. Further, we limited flash drought events to those that occurred in the period 2010–20 (Fig. 1). The specific flash drought events that met the criteria are summarized in Table 1.

The selected case studies provided a diverse set of conditions to investigate changes in VPD and soil moisture during extreme drydown events. During the flash drought event that occurred in the northern Great Plains in 2017, damage to agricultural production created losses exceeding $2.6 billion and seeded conditions for wildfires in Montana (Hoell et al. 2020; Smith 2020). It is

TABLE 1. Summary of study regions.

Region	Temporal period	Reference(s)
Northern Great Plains	Spring–summer 2017	Hoell et al. (2020), Wang et al. (2019)
Central United States	Spring–summer 2012	Otkin et al. (2016), Rippey (2015)
South-central United States	Summer–fall 2015	Otkin et al. (2019)
Southeast	Summer–fall 2016	Williams et al. (2017)

ranked as the second driest year of the period 1901–2017 (Wang et al. 2019). The 2012 flash drought devasted the central United States and led to $2 billion of losses from agriculture and $800 million from timber production (Otkin et al. 2016). Sustained high temperatures created severe moisture and heat stress throughout the central United States that persisted for the remainder of the growing season (Rippey 2015). In 2015, an extreme flash drought began in the summer after a relatively wet spring (Otkin et al. 2019). This event was unusual as it quickly recovered following a wet period in October. Finally, the 2016 flash drought event that affected the Southeast was driven by low precipitation and elevated temperatures that persisted for months (Williams et al. 2017), unlike the rapid onset and recovery observed in the 2015 event. This drydown event led to wildfires in the region and over $100 million in crop production losses.

The types and proportions of vegetation types represented in the study regions differ as determined by the North American Land Data Assimilation System (NLDAS) University of Maryland (UMD) land cover classification data (Fig. 1). The Southeast and south-central United States, which were regions impacted by the 2016 and 2015 flash drought events, respectively, are the most similar in terms of the types of vegetation present. Both areas are predominantly occupied by woodland and wooded grassland (50%). About 20% of each region is covered by cropland. Evergreen needleleaf forest is the fourth most prevalent land cover type in the south-central United States and fifth most prevalent in the Southeast. While both areas have 5% of the area classified as mixed forest, the Southeast has a much higher percentage of deciduous broadleaf forest (15.6%), whereas only 2.8% of the south-central United States is classified as such. The strong similarity between land cover compositions in these two regions can be attributed to significant overlap between the two areas (Fig. 1). This overlap, however, does not hinder the interpretation of further results as each study area represents a separate flash drought event.

The central United States, the largest study region, was devastated by the 2012 flash drought (Basara et al. 2019). This area is largely dominated by croplands (44.4%, Fig. 1). The next most prevalent land cover type is deciduous broadleaf forest (12.3%). Wooded grassland and grassland both occupy around 15% of the region. Woodland, mixed forest, and evergreen needleleaf forests make up small percentages of the total land cover in the central United States.

Urban areas constitute less than 1% of land cover in all regions (Fig. 1). The dominant land cover type in the northern Great Plains is grassland, which makes up the majority of the area (69.4%). The next most prevalent vegetation type is cropland (12.5%). Evergreen needleleaf, open shrubland, woodland, wooded grasslands, and open shrubland combined make up 18% of the remaining area in the northern Great Plains.

b. Data

Several datasets were leveraged to investigate the evolution of root-zone soil moisture and vapor pressure deficit across different land surface types during flash drought.

For flash drought identification, evapotranspiration (ET) and potential evapotranspiration (PET) were used from phase 2 of the NLDAS Noah-2.8 land surface model data (Xia et al. 2012). NLDAS-2 data have a spatial resolution of 0.125° and are provided hourly. For this study, NLDAS-2 ET and PET data from 1980 to 2020 were used.

In addition to the variables used for flash drought analysis, land cover and soil texture classification data provided in NLDAS-2 were used in this study. The NLDAS-2 land cover data were derived from the UMD land cover classification (Hansen et al. 2000). In the UMD classification scheme, 13 vegetation classes are included, with an additional class for water. Soil texture data on the NLDAS-2 grid were derived from the 1-km Pennsylvania State University STATSGO data (Miller and White 1998). The STATSGO dataset provided soil texture types in 16 classifications. A lookup table was used to determine soil hydraulic parameters based on soil texture (Table S1 in the online supplemental material). The Brooks–Corey and Campbell soil hydraulic parameters were used to determine the air-entry pressure head and porosity (Clapp and Hornberger 1978; Dingman 2015). Soil water infiltration parameters for suction front head and pore-size distribution followed from Rawls and Brakensiek (1982) and Rawls et al. (1991, 1992).

For modeling thresholds that define vegetation stress during flash drought, VPD was derived from the NLDAS-2 reanalysis data for meteorological fields at a 0.125° grid spatial resolution and an hourly temporal resolution (Xia et al. 2012). Surface temperature, pressure, and specific humidity were used to estimate daily VPD from the NLDAS-2 data 2010–20. Daily average VPD (kPa) was calculated as the difference between saturated e_{sat} and unsaturated e vapor pressure:

$$\mathrm{VPD} = e_{sat} - e, \tag{1}$$

where e (kPa) is calculated using daily averages of NLDAS-2 specific humidity q and surface pressure p (kPa),

$$e = q \times p/0.622, \tag{2}$$

and e_{sat} (kPa) is calculated using Tetens equation (Monteith and Unsworth 2013, p. 13)

$$e_{sat} = 0.611 \exp\left(\frac{17.27 \times T}{T + 237.15}\right), \tag{3}$$

where T (°C) is the daily average temperature derived from NLDAS-2.

Soil moisture data used in this study came from the Soil MERGE (SMERGE) root-zone soil moisture product (Tobin et al. 2019). This dataset provides root-zone soil moisture representing the 0–40-cm layer for the contiguous United States from NLDAS reanalysis merged with European Space Agency Climate Change Initiative satellite data. It is available at a daily temporal resolution and on the same 0.125° grid as NLDAS-2. SMERGE soil moisture θ is used to estimate soil

water potential ψ_{soil} (J kg^{-1}) via the Clapp and Hornberger equation

$$\psi_{soil} = \psi_{ae}\left(\frac{\theta}{\phi}\right)^{-b}, \quad (4)$$

where ψ_{ae} (J kg^{-1}) is the air-entry water potential, ϕ is the porosity, and b is an empirical parameter related to the pore-size distribution (Dingman 2015; Campbell 1974; Lai and Katul 2000; see also Table S1 in the supplemental material).

Vegetation phenology data for canopy greenness and density were obtained from the Moderate Resolution Imaging Spectroradiometer (MODIS) MOD15A2H v006 (Myneni et al. 2015). This satellite remote sensing product provides leaf area index (LAI) and fraction of photosynthetically active radiation (FPAR) at 8-day temporal resolution and 500-m spatial resolution. The data were bilinearly interpolated to the same 0.125° spatial grid as NLDAS-2.

c. *Determining thresholds for vegetation stress*

The Dynamic Canopy Biophysical Properties model (DCBP) was used to determine the range for suboptimal vegetation function for VPD and soil moisture using the method developed and validated by Lowman and Barros (2018). Lowman and Barros (2018) previously demonstrated that the DCBP model predicted changes in phenology consistent with MODIS FPAR and LAI observations and, when coupled to a land surface hydrology model, estimated photosynthesis rates that matched observations from eddy-covariance flux towers during wet and dry periods. The DCBP combines phenologic forecasting with data assimilation to estimate the environmental conditions under which photosynthesis operates. It consists of a phenology forecasting model based on the growing season index (GSI), which provides a unitless measure of the potential phenologic state of vegetation based on the concurrent meteorological conditions (Jolly et al. 2005). The GSI was previously validated against ground-based LAI measurements and long-term datasets of field observations of phenology (Jolly et al. 2005; Stöckli et al. 2008). It is framed as a multiplicative function that depends on conditions that affect plant growth and senescence, which are: minimum daily temperature (T_{min}), daylength (Pht), VPD, and soil water potential (ψ_{soil}) (Lowman and Barros 2018):

$$\mathrm{GSI} = f(T_{min}) \times f(\mathrm{Pht}) \times [1 - f(\mathrm{VPD})] \times f(\psi_{soil}). \quad (5)$$

The GSI and each of the multiplicative index functions are unitless and scaled between 0 and 1, where 0 means that the plant is no longer growing and 1 means that growth is uninhibited. Each function has the form

$$f(x) = \begin{cases} 0 & \text{if } x \le x_{min} \\ \dfrac{x - x_{min}}{x_{max} - x_{min}} & \text{if } x_{min} < x < x_{max}. \\ 1 & \text{if } x \ge x_{max} \end{cases} \quad (6)$$

The index functions for minimum daily temperature and daylength provide the timing of green-up and senescence and overall shape of the growing season, while VPD and soil water potential determine changes in canopy development during the growing season that result from water stress (Lowman and Barros 2018). In the index function, maximum VPD (VPD_{max}) and minimum soil moisture (SM_{min}) denote when plants shut down growth and photosynthetic activity due to water stress in the atmosphere and soil, respectively. It is critical to note that SM_{min} is distinct from and not always equivalent to wilting point, the point at which cavitation occurs and plants do not recover. Within the context of the GSI, the SM_{min} and VPD_{max} parameters are associated with stomatal closure (Jolly et al. 2005; Lowman and Barros 2018), which plants use to regulate photosynthetic activity and conserve water during drought (e.g., Zhou et al. 2013). The SM_{min} and SM_{max} parameters are defined at plot and larger spatial scales and incorporate information about soil texture, vegetation type, and climate. VPD_{min} and VPD_{max} will also aggregate vegetation response at the ecosystem scale. In a similar vein, Bassiouni et al. (2020) estimated thresholds of soil water potential that corresponded to a suboptimal range of soil water uptake relevant at ecosystem scales.

While the GSI provides a measure of potential phenologic state, current phenologic state P is determined by where current FPAR falls relative to its minimum FPAR_{min} and maximum FPAR_{max} values (Stöckli et al. 2008):

$$P = \frac{\mathrm{FPAR} - \mathrm{FPAR}_{min}}{\mathrm{FPAR}_{max} - \mathrm{FPAR}_{min}}. \quad (7)$$

A growth vector, ΔGSI, is then defined as the difference between the potential, GSI, and current P phenologic states (Lowman and Barros 2018; Stöckli et al. 2008). If ΔGSI is positive then vegetation is growing and if ΔGSI is negative, then vegetation is senescing. New leaf growth or loss, $\Delta\mathrm{FPAR}/\Delta t$, is determined by

$$\frac{\Delta\mathrm{FPAR}}{\Delta t} = \gamma \times \Delta\mathrm{GSI} \times P(1 - P), \quad (8)$$

where γ is a growth rate parameter that describes how quickly vegetation responds to environmental conditions, and $P(1 - P)$ enforces a logistic growth constraint. Once a new FPAR value is predicted for the next time step using Eq. (8), LAI is estimated from FPAR using Beer's law (Sellers et al. 1996):

$$\mathrm{LAI} = \frac{\ln(1 - \mathrm{FPAR})}{\ln(1 - \mathrm{FPAR}_{max})} \times \mathrm{LAI}_{max}. \quad (9)$$

An inverse modeling framework is used to estimate the parameters within the index functions that define the GSI. Specifically, the x_{min} and x_{max} values for $f(T_{min})$, $f(\mathrm{Pht})$, $f(\mathrm{VPD})$, and $f(\psi_{soil})$ are determined using an ensemble Kalman filter (EnKF) that jointly estimates the GSI parameters and the phenologic states of FPAR and LAI (Lowman and Barros 2018; Stöckli et al. 2008; Moradkhani et al. 2005). In this way we determine the minimum and maximum thresholds for VPD and soil water potential within the DCBP (Fig. S2), along with seven other parameters ($T_{min_{min}}$, $T_{min_{max}}$, Pht_{min}, Pht_{max}, γ, FPAR_{min}, and LAI_{max}). MODIS FPAR and LAI data are assimilated at an 8-day interval (the native temporal

resolution of the satellite product) to constrain and reduce error in predicted FPAR and LAI values and the GSI parameter estimates. The GSI parameters that define the range of suboptimal vegetation function are produced on a pixel-by-pixel basis at the 0.125° resolution of the NLDAS-2 spatial grid (Fig. S2). Validation of the DCBP model and the parameters estimated within to define vegetation phenologic response to environmental conditions was conducted for various AmeriFlux sites and documented in Lowman and Barros (2018). The specific parameters that are used in this study to indicate extreme vegetation stress (i.e., stunted growth or shutdown of photosynthesis) are maximum VPD and minimum soil water potential. Minimum soil water potential is converted to a minimum soil moisture threshold on a pixel-by-pixel basis using the Clapp and Hornberger equation [Eq. (4)] (Dingman 2015; Campbell 1974).

Onset of vegetation stress could be evaluated using minimum VPD and maximum soil water potential to characterize when atmospheric and soil conditions cause vegetation growth and photosynthesis to fall below their maximum. However, vegetation tends to spend a large part of the growing season within the suboptimal range of VPD and soil moisture defined by the minimum and maximum thresholds derived from the DCBP model (Lowman and Barros 2018; Stöckli et al. 2008). On the other hand, extreme drought conditions will lead to complete shutdown of growth and photosynthetic activity during the growing season. Thus, the thresholds that correspond to photosynthetic shutdown in the GSI provide clear, quantifiable negative outcomes that can be attributed to either VPD or soil moisture. Moving forward, we focus on evaluating when VPD and soil moisture exceed $\mathrm{VPD}_{\max}$ and/or fall below $\mathrm{SM}_{\min}$.

d. Flash drought identification

Flash drought events were detected using a modified framework for SESR from Christian et al. (2019b) and described in Christian et al. (2022). First, ET and PET were used to calculate the evaporative stress ratio (ESR), such that

$$\mathrm{ESR} = \frac{\mathrm{ET}}{\mathrm{PET}} \tag{10}$$

and ESR ranges from zero to approximately one. As ESR approaches one, the atmospheric demand for moisture is met by evapotranspiration at the land surface and evaporative stress on the environment is low. In contrast, ESR values approaching zero indicate that evapotranspiration from the land surface is meeting little or none of the atmospheric demand and high evaporative stress exists. To limit some of the volatility in daily ESR, 5-day (pentad) averages of ESR are then computed on a pixel-by-pixel basis. A pentad average is defined as the mean of 5 nonoverlapping days, and every year has 73 pentads. Pentad values of ESR are then standardized to more easily compare evaporative stress values across different climate regimes, years, and parts of the growing season. SESR is calculated as

$$\mathrm{SESR}_{ijp} = \frac{\mathrm{ESR}_{ijp} - \overline{\mathrm{ESR}_{ijp}}}{\sigma_{\mathrm{ESR}_{ijp}}}, \tag{11}$$

where SESR_{ijp} (henceforth referred to as SESR) is the z score of ESR for a specific pentad p at a specific grid point (i, j), $\overline{\mathrm{ESR}_{ijp}}$ is the mean ESR for a specific pentad p at a specific grid point (i, j) for all years available in the gridded dataset, and σ_{ESR} is the standard deviation of ESR for a specific pentad p at a specific grid point (i, j) for all years available in the gridded dataset.

To account for pentad-to-pentad variability in SESR, a Savitzky–Golay filter was used to smooth the time series while preserving higher moments in the data (Savitzky and Golay 1964). This filtering technique is advantageous compared to running averages, as moving statistical means calculated over large periods of time will smooth out subseasonal signals. Because rapid subseasonal declines in SESR occur during flash drought, it is critical to maintain these rapid transitions while reducing noise in the time series (Christian et al. 2022). Following guidance from the Savitzky–Golay filtering technique applied to remote sensing observations (Chen et al. 2004), $d = 4$ was used for the degree of polynomial, and $m = 10$ was used as the half-width of the smoothing window ($m = 10$ indicates 21 time steps and a 105 day smoothing window for pentad resolution data).

The change in SESR over time is used to capture rapid drought intensification. After the Savitzky–Golay filter was applied to the SESR time series, the derivative of SESR with respect to time was calculated as a forward difference between each pentad. The change in SESR is standardized in the same way as ESR

$$(\Delta\mathrm{SESR}_{ijp})_z = \frac{\Delta\mathrm{SESR}_{ijp} - \overline{\Delta\mathrm{SESR}_{ijp}}}{\sigma_{\Delta\mathrm{SESR}_{ijp}}}, \tag{12}$$

where $(\Delta\mathrm{SESR}_{ijp})_z$ (henceforth referred to as ΔSESR) is the z score of the change in SESR for a specific pentad p at a specific grid point (i, j), $\overline{\Delta\mathrm{SESR}_{ijp}}$ is the mean change in SESR values for a specific pentad p at a specific grid point (i, j) for all years available in the gridded dataset, and $\sigma_{\Delta\mathrm{SESR}_{ijp}}$ is the standard deviation of SESR for a specific pentad p at a specific grid point (i, j) for all years available in the gridded dataset.

The Savitzky–Golay filtering process applied to SESR allows for a simplified set of criteria from Christian et al. (2019b) to determine flash drought, outlined in Christian et al. (2022): 1) ΔSESR must be at or below the 25th percentile between individual pentads, 2) the final SESR value is below the 20th percentile of SESR values, and 3) the drydown event defined by criteria 1 and 2 must last at least 30 days (i.e., 6 total pentads or 5 ΔSESR periods), which defines a period of rapid land surface desiccation. The first criterion is used to capture the rapid rate of intensification toward drought, and the second and third criteria are used to emphasize impact and longevity, respectively, associated with drought and flash drought (Otkin et al. 2018). Onset of flash drought is defined as the first pentad in the SESR time series during which criterion 1 is satisfied.

SESR has been validated within the United States and globally over the past decade as a method for evaluating flash drought. SESR compares well with the satellite-derived ESI

(Christian et al. 2019b; Anderson et al. 2007a,b) and LSWI (Christian et al. 2022), acts as an early drought indicator, and corresponds with impacts indicated by the U.S. Drought Monitor (USDM; Christian et al. 2019b; Svoboda et al. 2002) and land surface desiccation via satellite observations (Christian et al. 2020). Further, it provides flash drought occurrence both regionally and nationally across the United States (Christian et al. 2019b,a) and represents the development and evolution of flash drought case studies using different datasets across different regions around the globe (Basara et al. 2019; Christian et al. 2020, 2021).

By using time series of SESR, which detects onset and evolution of flash drought, and of VPD and soil moisture along with their GSI-determined thresholds for suboptimal vegetation function, we determine which condition preceded the onset of rapidly deteriorating drought conditions.

3. Results

a. *Flash drought detection with SESR*

The four cases selected for this study allowed us to investigate flash drought development across various regions within the continental United States and with different onset timing during the growing season (Fig. 2). The first and perhaps most notable of these cases includes the 2012 flash drought across the central United States (Fig. 2a). Rapid drought intensification initially began in April across Kansas, then propagated eastward into the Midwest and northward within the central Great Plains during May and June. By July and August, flash drought development also initiated over the Great Lakes region. In 2015, flash drought developed across the south-central United States, with rapid drought intensification primarily in the middle of the growing season over southern Arkansas, Louisiana, and Mississippi (Fig. 2b). In addition, flash drought development occurred in September across portions of east Texas and Louisiana. Flash drought onset occurred late in the growing season across the Southeast in 2016, with development across large areas of Arkansas, Louisiana, Tennessee, Mississippi, Alabama, and Georgia (Fig. 2c). Timing of flash drought development generally occurred between August and October. The last case study includes the 2017 northern Great Plains flash drought. Rapid drought intensification developed early in the growing season, with Montana and western North Dakota experiencing flash drought primarily in April and May (Fig. 2d).

b. *Variability of flash drought classification by land cover type*

To determine whether certain land cover types are more susceptible to flash drought, we investigated the proportion of pixels classified as a specific vegetation type that experienced flash drought within the study area. If all land cover types were equally likely to be affected by drought, then we should see relatively equal proportions of each vegetation type affected by drought across the study areas. In other words, all vegetation types would be uniformly affected by drought regardless of their relative distributions within the area. Conversely, if a land cover type is more (less) susceptible to drought, then its proportion would be higher (lower) than the percentage of the overall area experiencing flash drought. The following paragraphs summarize our findings for which land cover types are responding anomalously to flash drought from the 2012, 2015, 2016, and 2017 case studies respectively.

In 2012, 82% of pixels within the central U.S. study region experienced flash drought as determined by SESR (Fig. 2a); however, a large spread was observed between land cover types in the percentage of pixels affected by flash drought (Fig. 3a). Cropland (94%) and wooded grassland (89%) land cover types were found to be overrepresented relative to the 82% of pixels overall that experienced flash drought in the central United States. Woodland vegetation (83%) was in line with what would be expected in the region in 2012. Meanwhile, the land cover types there that were found to be underrepresented included grassland (72%), deciduous broadleaf forest (66%), closed shrubland (33%), evergreen needleleaf forest (39%), and mixed forest (58%). Thus, the most dominant land cover type (cropland) in the central U.S. region was also its most vulnerable.

A modest 50% of pixels experienced a flash drought in the south-central U.S. domain in 2015 (Fig. 2b). Despite the fact that only 50% of the total area was affected by flash drought, there were still notable differences between land cover types (Fig. 3b). Evergreen needleleaf and croplands had over 50% of pixels experience flash drought and thus were overrepresented and more susceptible to flash drought in the south-central United States in 2015. Conversely, deciduous broadleaf forests (14%) and grasslands (10%) percentages fell well below the regional proportion where flash drought was detected, suggesting that these vegetation types were less susceptible to flash drought. The percentages of flash drought for mixed forests (45%), woodland (50%) and wooded grasslands (42%) were in line with the regional flash drought incidence rates.

Across the Southeast in 2016, a total of 49% of pixels in the region experienced flash drought (Fig. 2b). As with the other study regions, there was a large spread in the percentage of land cover types that experienced a flash drought. The following land cover types were considered overrepresented: cropland (75%) and woodland (57%) (Fig. 3b). Between 45% and 50% of wooded grassland and mixed forests experienced flash drought, which is around what would be expected if they were equally susceptible to drydown events. Fewer than 30% of evergreen needleleaf and deciduous broadleaf forests were affected by flash drought, suggesting that these vegetation types were less susceptible to flash drought in the Southeast.

The northern Great Plains in 2017 displays the most uniform behavior in how different land cover types are affected by flash drought (Fig. 3d). While the aerial percentage of pixels affected by flash drought is 57% (Fig. 2b), between 51% and 62% of all vegetation types experienced flash drought in this period (Fig. 3b). Thus, in the northern Great Plains, it appears that all land cover types are equally susceptible to flash drought. The one exception being evergreen needleleaf forests appear slightly more susceptible to flash drought than other vegetation types.

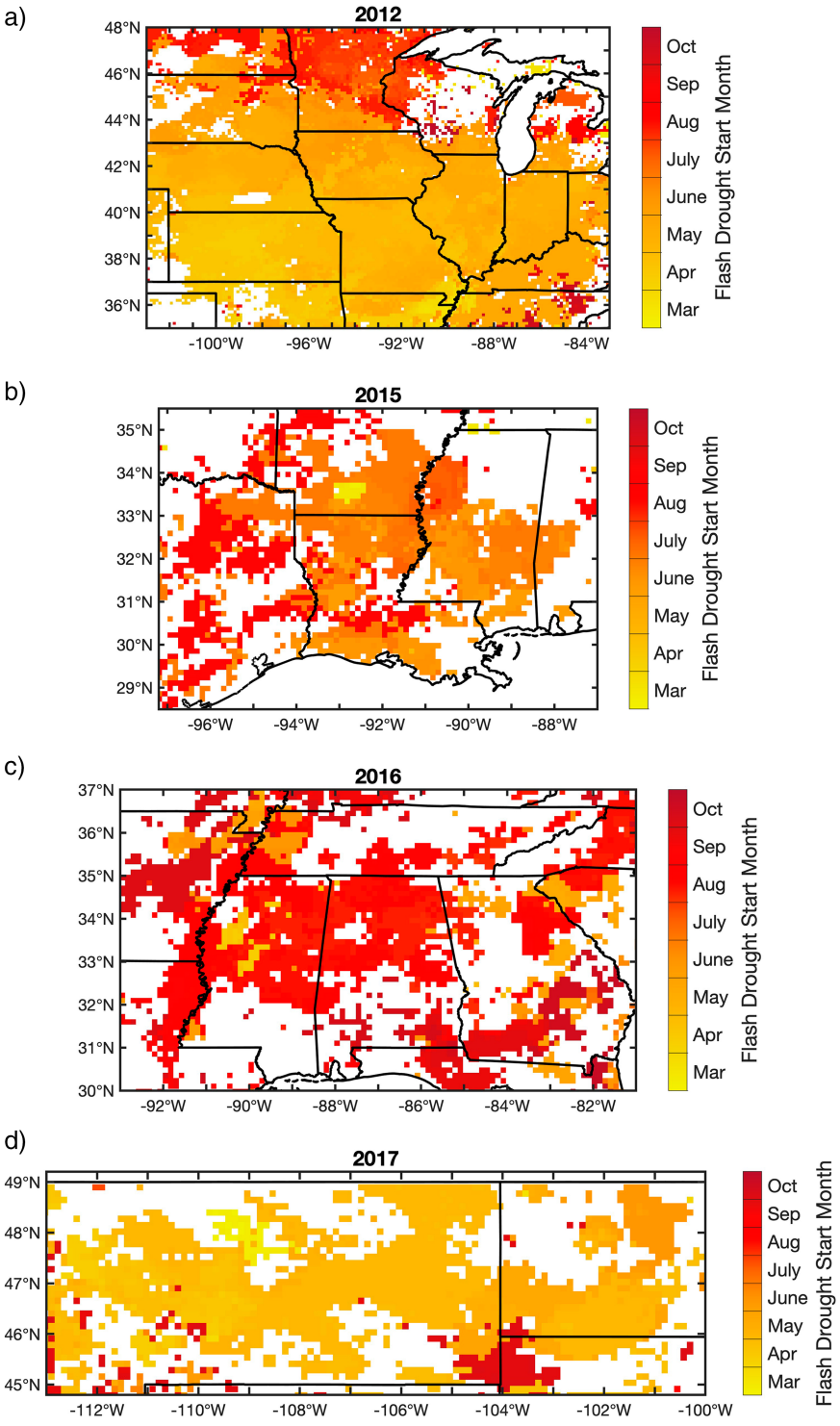

FIG. 2. Timing of flash drought development across (a) the central United States during 2012 (82.4% of domain experienced flash drought), (b) the south-central United States during 2015 (50.1% of domain experienced flash drought), (c) the Southeast during 2016 (49.4% of domain experienced flash drought), and (d) the northern Great Plains during 2017 (56.8% of domain experienced flash drought).

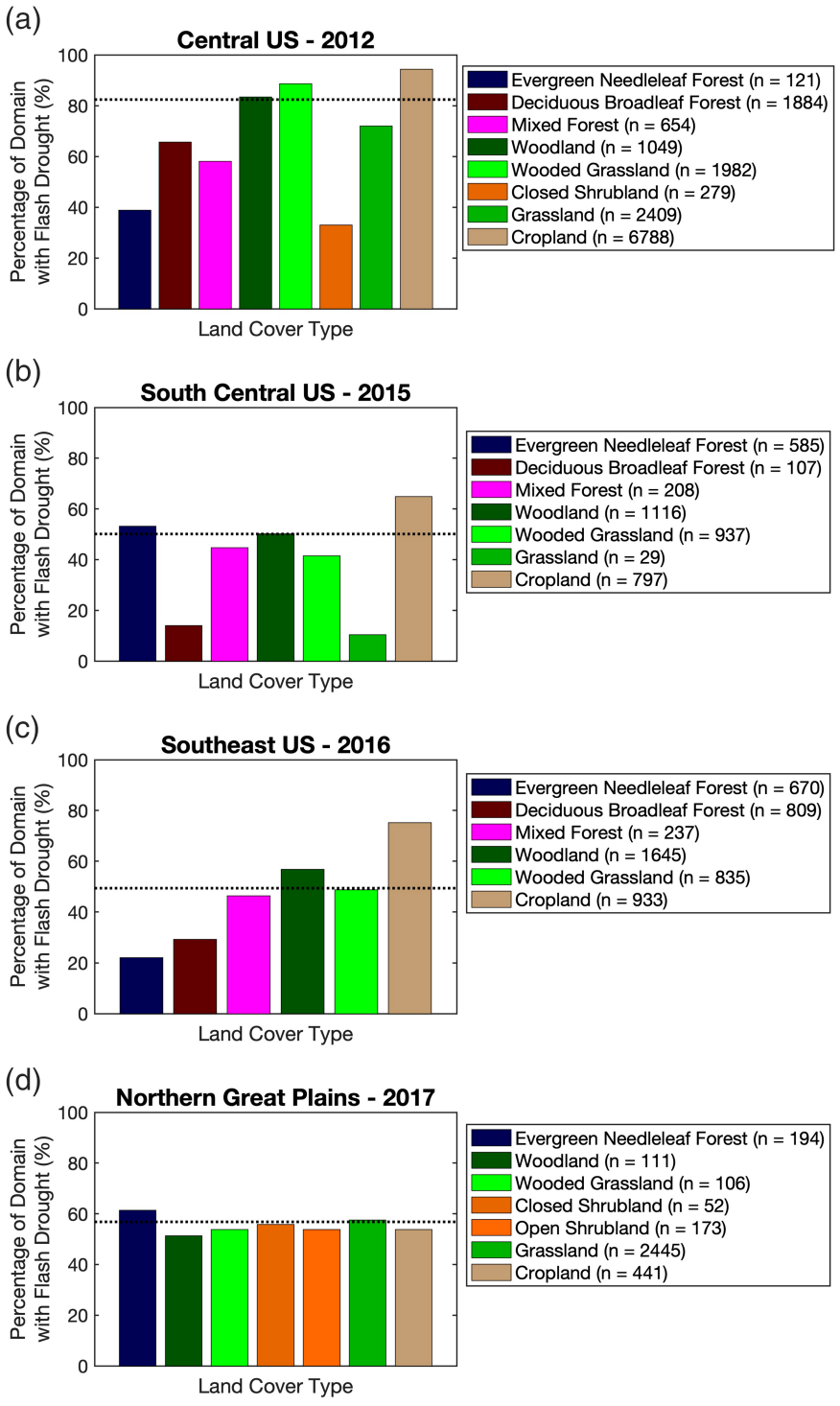

FIG. 3. Percentage of domain classified as a particular land cover type where flash drought was detected by SESR for each case study. The *n* value in the legend provides the total number of grid points assigned to the land cover type within the domain. The black dashed line represents the overall frequency of flash drought occurrence across the entire domain shown in Fig. 2. (a) Central United States, (b) south-central United States, (c) Southeast, and (d) northern Great Plains.

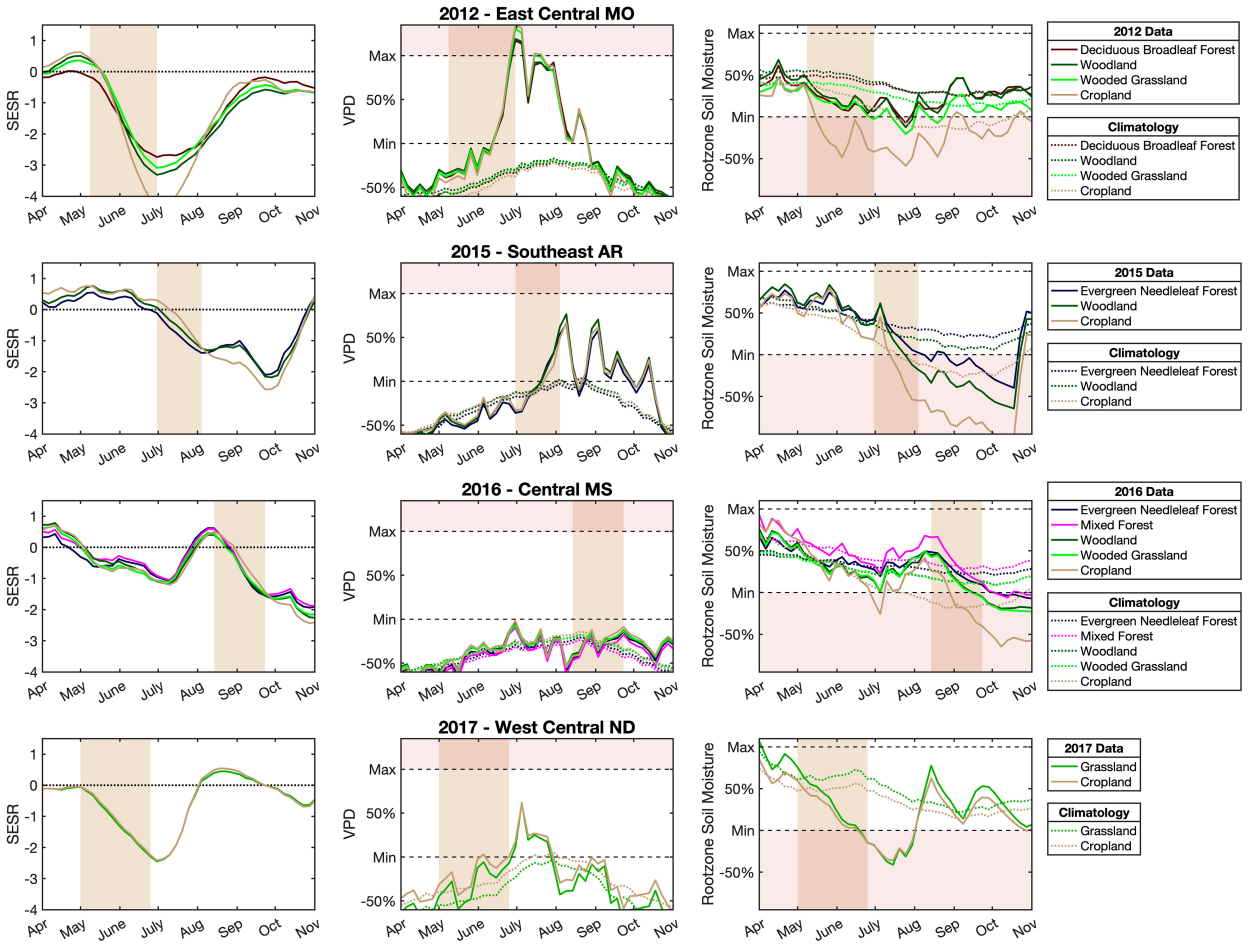

FIG. 4. (left) SESR derived from NLDAS-2, (center) VPD derived from NLDAS-2 and scaled between the minimum and maximum VPD thresholds that define the range between optimal photosynthesis and shutdown of plant activity, and (right) root-zone soil moisture from SMERGE and scaled between the minimum and maximum soil moisture thresholds that define the range between photosynthesis shut down and optimal for plant activity for selected grid points during flash drought development in (first row) east-central Missouri during 2012, (second row) southeast Arkansas during 2015, (third row) central Mississippi during 2016, and (fourth row) west-central North Dakota during 2017. Solid lines show the values of SESR, VPD, and root-zone soil moisture for individual pixels in each year. Dashed lines show the climatological average for each pixel between 1980 and 2020. The tan-shaded region shows the median timing for flash drought development for the selected pixels, and the red-shaded region highlights values of VPD and soil moisture where photosynthesis shuts down.

c. *Temporal evolution of land surface variables during flash drought*

To investigate how potential drivers of flash drought onset and progression may vary across different land cover types, we considered time series of atmospheric aridity (VPD) and soil moisture during rapid drought development over particular vegetation types within each study region (Fig. 4). Individual grid cells were selected where 1) flash drought occurred, 2) at least two or more land cover types are adjacent to each other, and 3) where VPD and soil moisture thresholds are similar (Fig. S2). We evaluated the time series of SESR, VPD, and soil moisture for each case study and compared them to their climatological averages (Fig. 4). In all cases, the climatological average for VPD was at or below the VPD_{min} threshold which defines the region where photosynthesis is uninhibited. The climatological averages for root-zone soil moisture fell largely in the range of suboptimal vegetation function (i.e., between SM_{min} and $SM_{max)}$, except for the climatological average soil moisture for croplands in the 2012, 2015, and 2016 case studies (Fig. 4). However, observed soil moisture fell well below the climatological average in each of these cases during flash drought.

In 2012 across east-central Missouri, flash drought initiated in early May and developed throughout the month of May and June (Fig. 4, row 1). Out of four selected grid cells in the region, the grid cell with the cropland land cover was documented to have the largest decline in SESR during the flash drought, while deciduous broadleaf forests had the least rapid decline in SESR. This suggests that croplands were more

strongly impacted by the flash drought in terms of evaporative stress as depicted by SESR. Toward the end of flash drought development at the end of June 2012, all vegetation types exceeded the maximum VPD (VPD_{max}) threshold above which photosynthesis shuts down, demonstrating the atmospheric moisture stress resulting from the flash drought. Root-zone soil moisture for the selected pixels show that cropland soil moisture dipped below the minimum threshold at which photosynthesis shuts down in May, only a couple of weeks into the flash drought event. The root-zone soil moisture for deciduous broadleaf, woodland, and wooded grassland pixels were reduced to below 25% during the period from June to August, and experienced shut down of photosynthesis in late July after the period of rapid drought intensification. This suggests that for east-central Missouri, the reductions in soil moisture were the primary driver for flash drought progression in 2012 for all vegetation types, while VPD compounded already dry conditions in late June and July.

In southeastern Arkansas during 2015, flash drought began in early July and occurred over a 4-week period through early August for grid cells with three different land cover types (Fig. 4, row 2). VPD remained below the VPD_{max} threshold for all vegetation types in 2015, suggesting that atmospheric aridity was not a primary driver for photosynthetic shutdown during this event. Root-zone soil moisture dropped below levels where photosynthesis shuts down for cropland pixels in mid-July (middle of flash drought development), for woodlands in early August (end of flash drought development period), and for evergreen needleleaf forests in early September (one month after flash drought event). Further, persistent soil moisture reductions led to worsening drought conditions in late August–October.

For selected grid cells across central Mississippi in 2016, below average SESR values were observed in May–July, but moisture conditions improved briefly between July and August before flash drought onset in mid-August (Fig. 4, row 3). VPD worsened for all vegetation types in late June, but remained below VPD_{min} suggesting that photosynthesis was not inhibited by atmospheric moisture stress during this flash drought event. Root-zone soil moisture dropped below the level where photosynthesis shuts down in early July for the cropland pixel. Soil moisture reductions below the minimum level in late August for croplands, early September for woodlands and wooded grasslands, and late September for evergreen needleleaf and mixed forests demonstrate the worsening drydown conditions.

In 2017, flash drought initiated in early May in west-central North Dakota and continued until late June (Fig. 4, row 4). Croplands and grasslands in this region experienced similar temporal trends in SESR, VPD, and soil moisture during this time. Soil moisture reduced below the minimum required for photosynthesis in mid-June and remained below the threshold until early August. Compounding this drydown in soils, VPD increased enough to reduce photosynthesis rates, but not enough to completely shutdown the gas exchange threshold in late June and early July.

d. VPD and soil moisture threshold exceedance of land surface variables

The prior results showed a localized example of VPD and soil moisture thresholds using a small subset of pixels within each study area. To consider how drying conditions in the atmosphere and soil are influenced by flash drought initiation and progression across the entire domains, we evaluated the percentage of land pixels that exceeded the VPD and soil moisture thresholds for photosynthetic shut down (Fig. 5).

In the central United States in 2012, few pixels exceeded thresholds for VPD (0%) and soil moisture (14%) one month prior to the flash drought event (Fig. 5a). One month after the flash drought event, 33% of pixels exceeded the VPD_{max} threshold and 67% of pixels exceeded the SM_{min} threshold. These results are consistent with what was observed with individual pixels in Fig. 4, where some vegetated pixels had dry soils before the flash drought event. A month after flash drought development, the majority of the central U.S. study region was experiencing soil moisture conditions severe enough to trigger a photosynthesis shutdown in plants. Atmospheric aridity affected a much smaller proportion of the study area, as 33% of the region had photosynthesis shutdown triggered by the VPD threshold.

In the south-central United States in 2015, a small percentage of pixels exceeded the VPD_{max} (1%) and SM_{min} (25%) thresholds prior to the flash drought event (Fig. 5b). One month after the flash drought developed, 0.5% of pixels exceeded the VPD_{max} threshold and 47% of pixels fell below the SM_{min} threshold. These results are consistent with what was observed for individual pixels in Fig. 4, where regardless of land cover type, few of the pixels exceeded the VPD_{max} threshold prior to or after the flash drought initiated. In the pixel-wise results, we also observed that the timing of crossing the SM_{min} threshold post flash drought development differed by land cover type, suggesting that this difference in timing could explain the near doubling of pixels experiencing soil moisture values below values for photosynthesis shut down one month after flash drought development.

In the Southeast in 2016, none of the vegetated pixels in the area exceeded the VPD_{max} threshold either in the month preceding or following flash drought development. Approximately 16% (43%) of pixels fell below the minimum soil moisture threshold before (after) flash drought development. This regional result is in line with what was observed for individual pixels in Fig. 4, where the VPD_{max} threshold was never crossed by any land cover type. Further, the cropland pixel crossed the soil moisture threshold prior to flash drought initiation, but all pixels representing distinct land cover types in the Southeast crossed this threshold following flash drought development. This difference in soil moisture threshold crossing before and after flash drought initiation suggests that the timing of the drydrown response is linked to land cover type.

In the northern Great Plains in 2017, no pixels exceeded the VPD_{max} threshold in the month prior to flash drought initiation, while 8% crossed the threshold in the month following flash drought development. Over 27% of pixels fell below the minimum soil moisture threshold in the month preceding

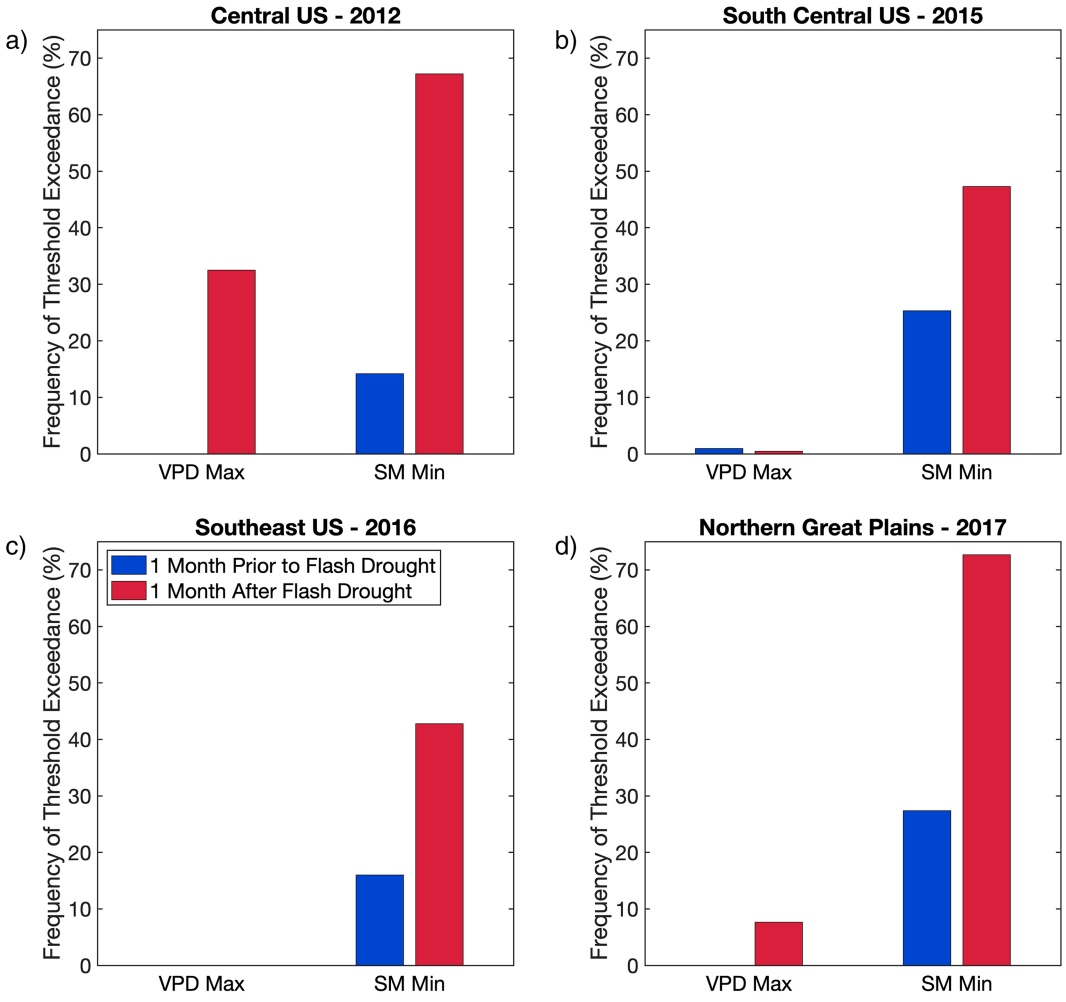

FIG. 5. Percentage of pixels that exceeded the thresholds of VPD and root-zone soil moisture prior to and after flash drought development for the four study regions: (a) central United States, (b) south-central United States, (c) Southeast, and (d) northern Great Plains.

the drought event, and 73% of pixels dropped below the minimum threshold after flash drought initiation. For the grassland and cropland pixels observed in Fig. 4, VPD did not exceed the VPD_{max} threshold, although it did increase, after flash drought initiation. Both pixels fell below the minimum soil moisture threshold following flash drought development.

e. *VPD and soil moisture threshold exceedance by land cover type*

We investigated how crossing thresholds indicating plant stress varied by land cover type within each study region. In the central United States in 2012, 61% of grassland and 52% of cropland pixels exceeded the VPD_{max} threshold during this period, which is at the high end relative to all other land cover types within this area (Fig. 6a). For wooded grasslands, 35% of pixels and for all other land cover types fewer than 17% of pixels crossed the VPD_{max} threshold. Approximately 88% of cropland pixels fell below the SM_{min} threshold after the flash drought event. Between 63% and 67% of grassland and wooded grassland pixels fell below the soil moisture threshold. Woodlands and closed shrublands had around 41%–43% of pixels cross the SM_{min} threshold. Evergreen needleleaf, deciduous broadleaf, and mixed forests had fewer than 17% of pixels cross the SM_{min} threshold.

In the south-central United States in 2015, approximately 0% of pixels of any land cover type exceeded the VPD_{max} threshold, suggesting that photosynthesis shutdown due to high VPD did not occur. On the other hand, soil moisture fell below the SM_{min} threshold where photosynthesis shuts down. One-hundred percent of grassland pixels ($n = 3$) exceeded the soil moisture threshold, although this is a very small sample of pixels (Fig. 6b). Ninety-seven percent of cropland pixels fell below the SM_{min} threshold. Around 41% of wooded grassland pixels fell below the SM_{min} threshold. Between 16% and 28% of evergreen needleleaf, deciduous broadleaf, mixed forest and woodland pixels crossed the SM_{min} threshold.

For every land cover type in the Southeast in 2016, virtually none of the pixels exceeded the VPD_{max} threshold, suggesting

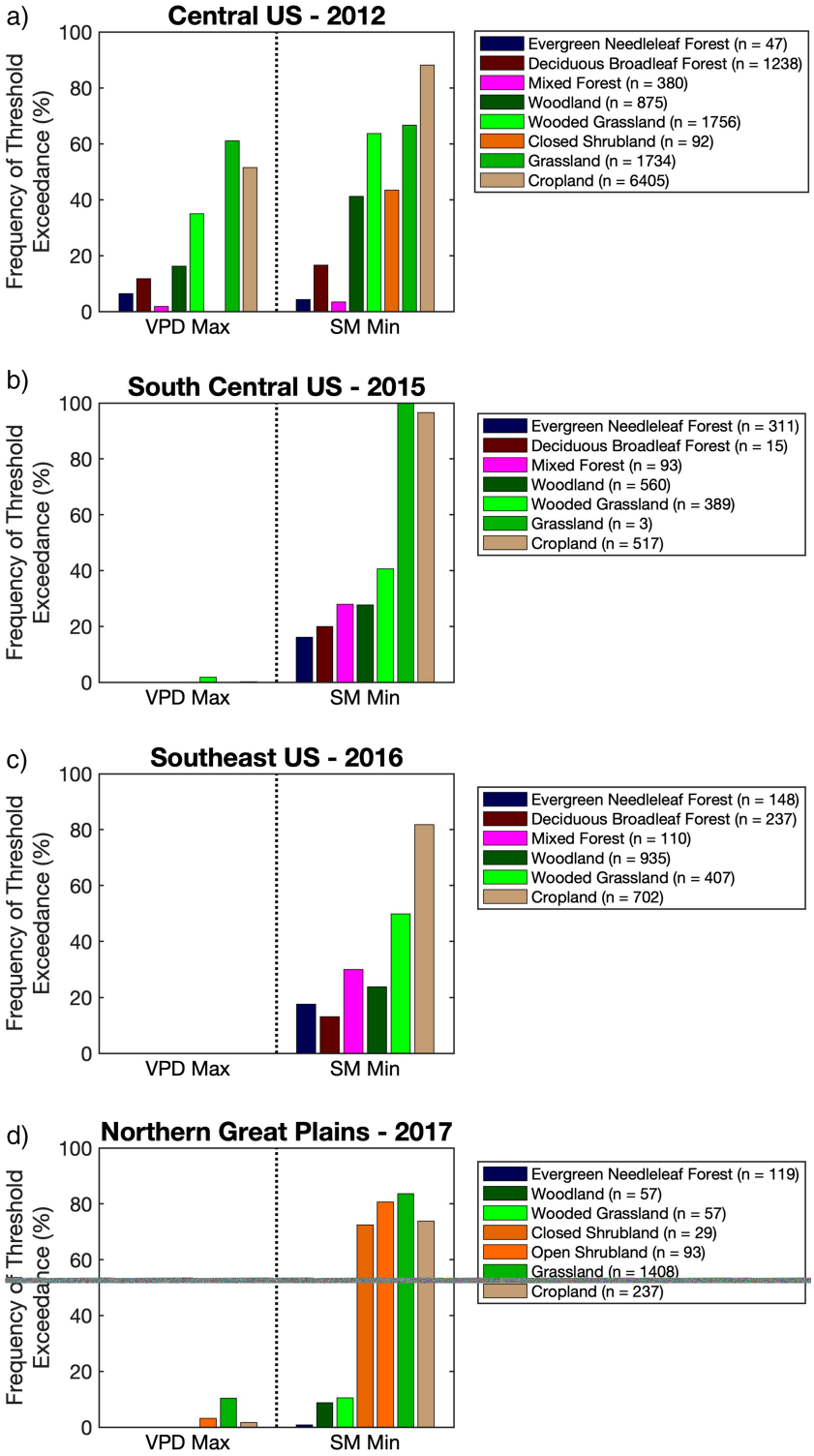

FIG. 6. Percentage of pixels representing different land cover types that exceeded the thresholds of VPD and root-zone soil moisture after flash drought development for the four study regions: (a) central United States, (b) south-central United States, (c) Southeast, and (d) northern Great Plains. The *n* value in the legend provides the total number of grid points that experienced flash drought within the domain for each land cover type.

that aridity in the atmosphere linked to flash drought events is not extreme enough to shutdown photosynthesis (Fig. 6c). On the other hand, nearly 82% of cropland pixels experienced soil moisture stress as demonstrated by soil moisture falling below the SM_{min} threshold. Approximately 50% of wooded grassland and 24% of woodlands crossed the SM_{min} threshold. Overall, a low percentage of pixels representing forested areas experienced soil moisture conditions that shutdown photosynthesis in the Southeast–30% of mixed forest, 18% of evergreen needleleaf, and 13% of deciduous broadleaf forests experienced soil moisture values below the SM_{min} threshold after flash drought onset.

In the northern Great Plains in 2017, fewer than 11% of grassland, open shrubland, and cropland pixels exceeded the VPD_{max} threshold, while none of the other land cover types were affected by atmospheric aridity (Fig. 6d). Eighty to eighty-four percent of grassland and open shrubland pixels experienced soil moisture levels below the SM_{min} threshold signaling shutdown of plant activity, while 72%–74% of cropland and closed shrubland pixels experienced similar conditions. Conversely, fewer than 11% of evergreen needleleaf, woodland, and wooded grassland pixels crossed the SM_{min} thresholds.

4. Discussion

a. *Regional differences in land surface response to flash drought*

In this study, we evaluated how soil moisture and VPD anomalies coevolved over different land cover types in four distinct regions of the United States. The most extensive flash drought occurred in 2012 across the central United States (Otkin et al. 2016). Over 82% of the region experienced a flash drought (Fig. 2), and most of the drought-affected pixels experienced low root-zone soil moisture values that fell below the SM_{min} threshold (Fig. 7). The extreme drydown conditions experienced during the 2012 flash drought are demonstrated by the fact that large portions of the region experience compounded effects of low soil moisture and high aridity that negatively impacted vegetation, namely in Oklahoma, Kansas, Missouri, Nebraska, Iowa, and South Dakota. This region also included subareas where only VPD worsened to above the VPD_{max} threshold in portions of Nebraska, Oklahoma, Iowa, and Missouri (Fig. 7). These results agree with previous findings that evaluating daily-scale variations in VPD and soil moisture during drought decouples their effects on vegetation response (Kimm et al. 2020; Novick et al. 2016).

In all case studies, at least 45% of the land area underwent flash drought (Fig. 2). During the 2017 flash drought in the northern Great Plains, the majority of the area fell below the minimum soil moisture threshold, and a smaller portion was triggered by both extremes in soil moisture and aridity (Fig. 7). In the south-central and southeastern U.S. regions, the vast majority of the drought-affected locations saw negative vegetation impacts triggered by low soil moisture (Figs. 6 and 7. Low soil moisture was found to be the primary driver in areas with irrigated croplands (i.e., along the Mississippi Delta) and where little to no irrigation takes place (i.e., in Alabama and eastern Tennessee). Both the 2015 and 2016 flash drought events initiated in late summer and early fall (Otkin et al. 2019; Williams et al. 2017), which may explain why these events observed relatively smaller regions where conditions for vegetation completely deteriorated.

b. *Sensitivity of vegetation to soil moisture and vapor pressure deficit*

Differences in how vegetation responded to worsening VPD and soil moisture conditions were observed within and across regions. Croplands were found to be susceptible to flash drought in all regions (Fig. 3). In almost all case studies, croplands demonstrated higher predisposition to flash drought, except for the 2017 flash drought event in the northern Great Plains where all land cover types were of near equal vulnerability for experiencing flash drought. We found that croplands tended to be the more vulnerable to flash drought compared to other plant functional types because they generally experienced a more rapid and sustained drop in soil moisture below the minimum threshold (Fig. 4). The modest exception to this was over the northern Great Plains region, where croplands and grasslands experienced similar worsening soil conditions. Our results align with prior work that demonstrated how croplands in the central United States have become increasingly sensitive to drought (Lobell et al. 2014). This result is particularly important because of the substantial economic impact of drought-induced losses on crop yields (Otkin et al. 2016).

Rooting depth likely plays a key role in determining how rapidly and for how long soil moisture conditions worsen across different vegetation types (Cui et al. 2019). Trees have deeper maximum rooting depths (7 m on average) than shrubs (5 m), herbaceous plants (3.5 m), and croplands (2.25 m) (Canadell et al. 1996), allowing them to access deeper stores of water during drought. We found forested areas to be less susceptible to enhanced dryness in soils and the atmosphere across all regions, while croplands and grasslands demonstrated higher susceptibility (Figs. 4 and 6). This finding aligns with Zhang and Yuan (2020), who found that vegetation responded rapidly to drying soil conditions and forests tended to have a higher resilience to flash drought using data collected from 29 FLUXNET stations.

Overall, we found that soil moisture was the dominant driver of flash drought across all vegetation types and in all case studies except for the 2012 event. This result aligns with prior studies that also found soil moisture, rather than VPD, to be a dominant driver of negative vegetation impacts (e.g., Liu et al. 2020; Zhou et al. 2019). Compound drought events, where both soil moisture and VPD extremes coevolve, are associated with the most extreme drought conditions (Zhou et al. 2019). As the most extreme flash drought event, in the 2012 case study we found both VPD and soil moisture were compounded drivers (Figs. 4, 6, and 7).

While previous studies have quantified the SM and VPD response during flash drought development, limited research has examined how these responses change across different land cover types. Throughout all four regions there was a general pattern with SM and VPD thresholds being exceeded

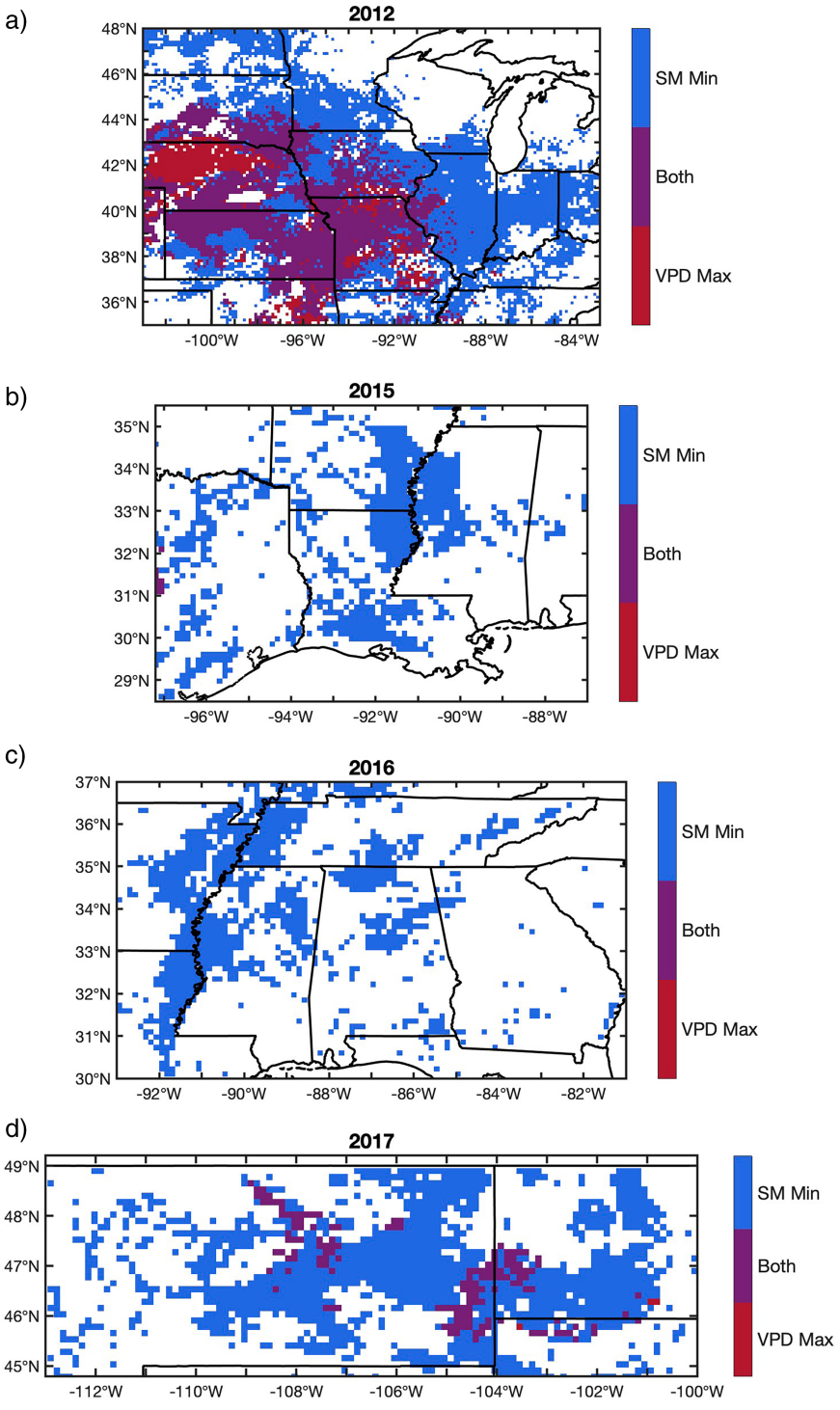

FIG. 7. Maps of locations that exceeded thresholds of VPD (red), root-zone soil moisture (blue), or both (purple) prior to or after flash drought development for the four study regions: (a) central United States, (b) south-central United States, (c) Southeast, and (d) northern Great Plains.

within a month of the initiation of flash drought, with clear spread of rapid drying across the regions (Fig. 5). The difference in timing of the SM and VPD threshold crossing varied by land cover. For example, the decline in soil moisture was generally much more rapid in areas with cropland than for pixels with other land cover types. The exception was across the northern Great Plains where the decline in soil moisture over grassland pixels was equivalent to that of the cropland pixels. Conversely, some land cover types appeared less vulnerable to flash drought. Perhaps the best example was across the central United States in 2012 where pixels with forested land cover (deciduous broadleaf, evergreen needleleaf, and mixed) experienced markedly less rapid decline in soil moisture and more modest levels of VPD compared to the more dominant cropland cover (Fig. 4, row 1). This pattern of forests being less vulnerable to flash drought development was similar in all regions (Fig. 6), regardless of the prominence of that land cover type.

One of the primary objectives in this paper was to determine the relative contribution of atmospheric aridity and soil moisture in driving negative vegetation impacts during flash drought events. What distinguished this approach from prior studies is that we considered how vegetation phenologic response (i.e., how the plant growth cycle is disturbed), rather than canopy conductance (Kimm et al. 2020), stomatal conductance and ET (Novick et al. 2016), and transpiration and photosynthesis (Sulman et al. 2016). This is important because vegetation phenology scales transpiration and photosynthesis rates govern land–atmosphere interactions. Results were mixed. Across the southeastern and south-central United States, which are more humid and where forest cover is more prominent, a relatively low percentage of pixels exceeded the VPD_{max} threshold. In those cases, soil moisture deficits tended to drive changes in vegetation development. Conversely, across the northern Great Plains region, where only a very small percentage of pixels have forested land cover (Fig. 1), soil moisture was the dominant driver (Fig. 6c). Pixels with cropland were generally the most vulnerable to flash drought. In all regions, the majority of cropland pixels fall below the SM_{min} threshold after flash drought onset; however, the VPD_{max} threshold was exceeded for 50% of croplands and 60% of grasslands after flash drought onset in the central United States, and to a lesser extent in the northern Great Plains (Fig. 6). This suggests that increased atmospheric aridity alone may only weakly inhibit photosynthesis activity during flash drought in regions dominated by forests (Fig. 6) and that croplands are uniquely vulnerable to flash drought. Christian et al. (2020) also demonstrated that the forested region in northern Russia had less negative values of SESR than regions to the south dominated by croplands.

c. Timing of flash drought

Finally, the timing of the onset of flash drought varied across the selected study regions: A majority of the land area in the central United States (2012) and northern Great Plains (2017) had an onset in May or June whereas a majority of the land area in the Southeast (2016) had an onset in August or September (Fig. 2). The difference in timing of flash drought onset plays a role in how severely vegetated areas are impacted (Lowman and Barros 2016, 2018; Zhang and Yuan 2020). The 2012 and 2017 flash droughts occurred early in the growing season, leading to devastating outcomes for vegetation that were largely driven by severe dry soil conditions during summer months (Fig. 4; Otkin et al. 2016; Hoell et al. 2020). The 2015 and 2016 flash droughts initiated later in the growing season (Fig. 4). Poor soil moisture conditions were observed late in the summer in 2015 and impacts on vegetation were minimal until later in the growing season. The unusual sequence of flash drought onset in July and flash recovery in October is evident in the evolution of SESR, VPD, and soil moisture (Fig. 4; Otkin et al. 2019). In 2016, flash drought onset occurred late in the summer and led to low soil moisture that stressed vegetation into the fall (Fig. 4; Williams et al. 2017).

Changes in subsurface and atmospheric moisture conditions prior to the onset of flash drought and after the period of flash drought development were evident in all four cases (Fig. 8). Soil moisture conditions were near normal or above normal before flash drought in each case, with the median soil moisture anomaly ranging between −0.01 and.02. However, soil moisture anomalies decreased well below normal following rapid drought development (median values between −0.03 and −0.06). The rapid depletion of soil moisture is also consistent with the response seen in other flash drought case studies (Hunt et al. 2014; Otkin et al. 2016; Ford et al. 2015). Further, as the environment transitions from energy-limited conditions to water-limited conditions during flash drought due to a reduction in soil moisture and ET (Otkin et al. 2018), the vapor pressure deficit will increase. This is evident in each of the four study regions with the median VPD increasing after flash drought development (an increase in the median VPD of 0.8 kPa in 2012, 0.3 kPa in 2015, 0.3 kPa in 2016, and 0.2 kPa in 2017). The increase in VPD has also been seen in other flash drought events, such as the flash drought in 2000 across eastern Oklahoma and western Arkansas (Otkin et al. 2013) and the 2010 flash drought over western Russian (Christian et al. 2020).

d. Limitations and considerations

The land cover dataset used in this study is the NLDAS-2 land cover classification, which does not distinguish between irrigated and rainfed crops (Hansen et al. 2000). Hunt et al. (2014) observed differences in irrigated and rainfed maize crops located at University of Nebraska–Lincoln (UNL) Agricultural Research and Development Center. Specifically, the study found that once root-zone soil moisture was depleted at the rainfed site, there was a significant difference in effects of water stress between irrigated and rainfed. However, complete depletion of root-zone soil moisture is more extreme than what was observed in any of the flash drought events evaluated in this manuscript. Additionally, the largest irrigated area evaluated in Hunt et al. (2014) was 65.4 ha (or approximately 800 m × 800 m), which is significantly smaller than the grid resolution of NLDAS used in this study (12.5 km × 12.5 km).

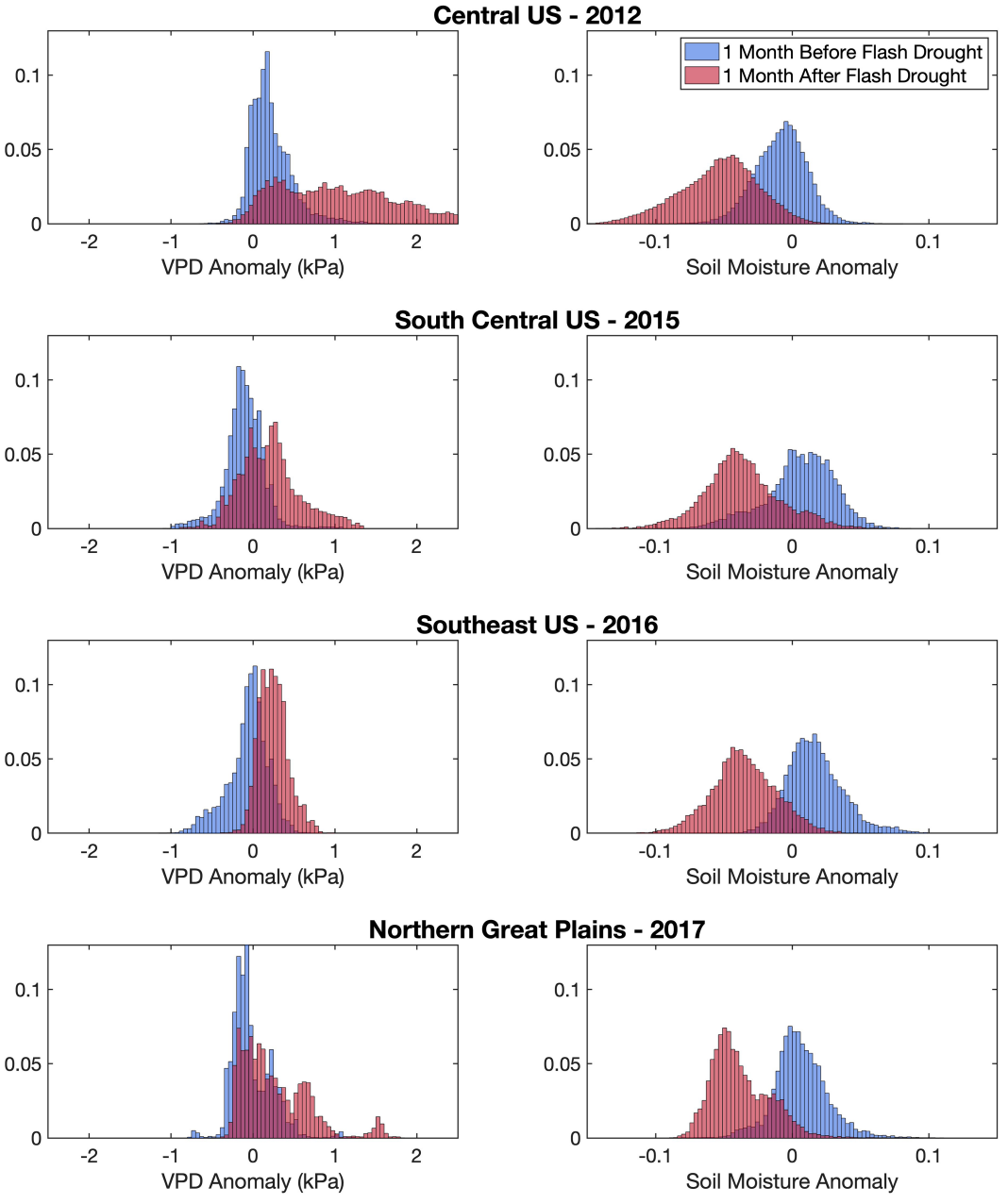

FIG. 8. VPD and root-zone soil moisture anomalies prior to and after flash drought development for the four study regions: (first row) central United States, (second row) south-central United States, (third row) Southeast, and (fourth row) northern Great Plains.

The SMERGE data product used for root-zone soil moisture in this study was previously validated in situ observations of soil moisture from sites that may have been influenced by irrigation practices. SMERGE soil moisture estimates perform as well as satellite remote sensing of soil moisture from SMAP (Tobin et al. 2019), which would include any signal from irrigation.

Reanalysis data for ET, PET, VPD, and root-zone soil moisture were selected because the data are available continuously for all study regions and at all time periods investigated from the NLDAS-2 and SMERGE datasets. As modeled products, we acknowledge that the datasets introduced some model error into the analysis. In terms of determining the thresholds for VPD_{max} and SM_{min}, these parameters are estimated by assimilating predictions of vegetation phenologic state defined by FPAR and LAI from DCBP model to MODIS observations. This step should reduce model error introduced by uncertainty and/or bias in the reanalysis datasets (Lowman and Barros 2018; Stöckli et al. 2008; Moradkhani et al. 2005). Individually, the reanalysis products represent well conditions

observed on the ground. SMERGE root-zone soil moisture has been shown to capture ecological effects when evaluated against NDVI from satellite remote sensing (Osman et al. 2021). Further, VPD derived from NLDAS compares well against in situ measurements (Fig. S3). And when SMERGE soil moisture and NLDAS VPD cross the thresholds determined for suboptimal plant function, this corresponds well with periods of reduced in situ photosynthesis rates for an AmeriFlux site located in the central United States during the 2012 flash drought (Fig. S3).

The approach to focus on crossing thresholds of VPD and soil moisture associated with photosynthetic shutdown was chosen because it provided a clear and quantifiable way to connect flash drought onset and evolution to negative land surface outcomes. However, this approach will not capture cases where VPD or soil moisture were very close to, but not yet crossing the thresholds. Such instances are also associated with severely reduced photosynthesis rates (e.g., Lowman and Barros 2018). For this reason, the time series of selected pixels before, during, and after flash drought onset were included to evaluate whether VPD and soil moisture could cause stress to plant function without complete shutdown (Fig. 4). In east-central Missouri (2012) and southeastern Arkansas (2015), both VPD and soil moisture are approaching thresholds for shutdown during flash drought onset. In east-central Missouri, the cropland crosses the SM_{min} threshold before crossing VPD_{max}; however, all other land cover types cross VPD_{max} in July before crossing SM_{min} in August (Fig. 4). In the 2012 case in east-central Missouri, all land cover types cross the SM_{min} threshold during flash drought onset and approach the VPD_{max} threshold without crossing it (Fig. 4). Thus, in both cases high VPD and low soil moisture are both contributing to reduced photosynthesis during the flash drought. While the approach could also be used to evaluate different discrete values of VPD and soil moisture associated with plant water stress during drought, for this study we were only interested in the most extreme cases that led to complete shutdown.

5. Conclusions

In this study, we investigated regional and land-cover-specific differences in how flash drought contributes to plant water stress through changes in VPD and soil moisture. Our results demonstrated that croplands and grasslands were more susceptible to deteriorating soil and atmospheric conditions, while forested areas were less vulnerable. In the four case studies investigated, soil moisture was found more consistently to lead to negative impacts on vegetation. Only in the most extreme drought event, the flash drought of 2012, were the compound effects of crossing both thresholds for VPD and soil moisture observed. This work provided a clear way to evaluate the primary drivers of vegetation stress during extreme drought events. The findings presented in this study provides information to land managers on which vegetation types in their region are more susceptible to extreme drought, and whether low soil moisture or elevated VPD is likely to lead to deterioration of vegetation conditions during these events. Future research should consider a climatology of flash drought events and threshold crossing to more rigorously determine the likelihood of extreme drought occurring for certain land cover types, spurred on by either VPD, soil moisture, both, or other environmental conditions.

Acknowledgments. This work was supported by the National Science Foundation (NSF) Division of Earth Sciences under NSF-2228047 and partially supported by internal funding from Wake Forest University.

Data availability statement. Data analyzed in this study were a reanalysis of existing data, which are openly available at locations cited in the reference section. Data generated by the DCBP model (Lowman and Barros 2018) are available upon publication as a Dryad database (https://doi.org/10.5061/dryad.stqjq2c6g). SESR data used in this study are included in Christian et al. (2022).

REFERENCES

Anderson, M. C., J. M. Norman, J. R. Mecikalski, J. A. Otkin, and W. P. Kustas, 2007a: A climatological study of evapotranspiration and moisture stress across the continental United States based on thermal remote sensing: 1. Model formulation. *J. Geophys. Res.*, **112**, D10117, https://doi.org/10.1029/2006JD007506.

——, ——, ——, ——, and ——, 2007b: A climatological study of evapotranspiration and moisture stress across the continental United States based on thermal remote sensing: 2. Surface moisture climatology. *J. Geophys. Res.*, **112**, D11112, https://doi.org/10.1029/2006JD007507.

Basara, J. B., J. I. Christian, R. A. Wakefield, J. A. Otkin, E. H. Hunt, and D. P. Brown, 2019: The evolution, propagation, and spread of flash drought in the central United States during 2012. *Environ. Res. Lett.*, **14**, 084025, https://doi.org/10.1088/1748-9326/ab2cc0.

Bassiouni, M., S. P. Good, C. J. Still, and C. W. Higgins, 2020: Plant water uptake thresholds inferred from satellite soil moisture. *Geophys. Res. Lett.*, **47**, e2020GL087077, https://doi.org/10.1029/2020GL087077.

Campbell, G. S., 1974: A simple method for determining unsaturated conductivity from moisture retention data. *Soil Sci.*, **117**, 311–314, https://doi.org/10.1097/00010694-197406000-00001.

Canadell, J., R. Jackson, J. Ehleringer, H. Mooney, O. Sala, and E.-D. Schulze, 1996: Maximum rooting depth of vegetation types at the global scale. *Oecologia*, **108**, 583–595, https://doi.org/10.1007/BF00329030.

Chen, J., P. Jönsson, M. Tamura, Z. Gu, B. Matsushita, and L. Eklundh, 2004: A simple method for reconstructing a high-quality NDVI time-series data set based on the Savitzky–Golay filter. *Remote Sens. Environ.*, **91**, 332–344, https://doi.org/10.1016/j.rse.2004.03.014.

Chen, L., T. W. Ford, and P. Yadav, 2021: The role of vegetation in flash drought occurrence: A sensitivity study using Community Earth System Model, version 2. *J. Hydrometeor.*, **22**, 845–857, https://doi.org/10.1175/JHM-D-20-0214.1.

Christian, J. I., J. B. Basara, J. A. Otkin, and E. D. Hunt, 2019a: Regional characteristics of flash droughts across the United States. *Environ. Res. Commun.*, **1**, 125004, https://doi.org/10.1088/2515-7620/ab50ca.

——, ——, ——, ——, R. A. Wakefield, P. X. Flanagan, and X. Xiao, 2019b: A methodology for flash drought identification: Application of flash drought frequency across the United States. *J. Hydrometeor.*, **20**, 833–846, https://doi.org/10.1175/JHM-D-18-0198.1.

——, ——, E. D. Hunt, J. A. Otkin, and X. Xiao, 2020: Flash drought development and cascading impacts associated with the 2010 Russian heatwave. *Environ. Res. Lett.*, **15**, 094078, https://doi.org/10.1088/1748-9326/ab9faf.

——, ——, ——, ——, J. C. Furtado, V. Mishra, X. Xiao, and R. M. Randall, 2021: Global distribution, trends, and drivers of flash drought occurrence. *Nat. Commun.*, **12**, 6330, https://doi.org/10.1038/s41467-021-26692-z.

——, ——, L. E. L. Lowman, X. Xiao, D. Mesheske, and Y. Zhou, 2022: Flash drought identification from satellite-based land surface water index. *Remote Sens. Appl.*, **26**, 100770, https://doi.org/10.1016/j.rsase.2022.100770.

Clapp, R. B., and G. M. Hornberger, 1978: Empirical equations for some soil hydraulic properties. *Water Resour. Res.*, **14**, 601–604, https://doi.org/10.1029/WR014i004p00601.

Crausbay, S. D., and Coauthors, 2017: Defining ecological drought for the twenty-first century. *Bull. Amer. Meteor. Soc.*, **98**, 2543–2550, https://doi.org/10.1175/BAMS-D-16-0292.1.

Cui, Z., G.-L. Wu, Z. Huang, and Y. Liu, 2019: Fine roots determine soil infiltration potential than soil water content in semi-arid grassland soils. *J. Hydrol.*, **578**, 124023, https://doi.org/10.1016/j.jhydrol.2019.124023.

Dingman, S. L., 2015: *Physical Hydrology*. 3rd ed. Waveland Press, 643 pp.

Dirmeyer, P. A., 2011: The terrestrial segment of soil moisture–climate coupling. *Geophys. Res. Lett.*, **38**, L16702, https://doi.org/10.1029/2011GL048268.

Edris, S. G., J. B. Basara, J. I. Christian, E. D. Hunt, J. A. Otkin, S. T. Salesky, and B. G. Illston, 2023: Analysis of the critical components of flash drought using the standardized evaporative stress ratio. *Agric. For. Meteor.*, **330**, 109288, https://doi.org/10.1016/j.agrformet.2022.109288.

Ford, T. W., and C. F. Labosier, 2017: Meteorological conditions associated with the onset of flash drought in the eastern United States. *Agric. For. Meteor.*, **247**, 414–423, https://doi.org/10.1016/j.agrformet.2017.08.031.

——, D. B. McRoberts, S. M. Quiring, and R. E. Hall, 2015: On the utility of in situ soil moisture observations for flash drought early warning in Oklahoma, USA. *Geophys. Res. Lett.*, **42**, 9790–9798, https://doi.org/10.1002/2015GL066600.

Fu, Z., and Coauthors, 2022: Atmospheric dryness reduces photosynthesis along a large range of soil water deficits. *Nat. Commun.*, **13**, 989, https://doi.org/10.1038/s41467-022-28652-7.

Gerken, T., G. T. Bromley, B. L. Ruddell, S. Williams, and P. C. Stoy, 2018: Convective suppression before and during the United States northern Great Plains flash drought of 2017. *Hydrol. Earth Syst. Sci.*, **22**, 4155–4163, https://doi.org/10.5194/hess-22-4155-2018.

Hansen, M. C., R. S. Defries, J. R. G. Townshend, and R. Sohlberg, 2000: Global land cover classification at 1 km spatial resolution using a classification tree approach. *Int. J. Remote Sens.*, **21**, 1331–1364, https://doi.org/10.1080/014311600210209.

He, M., J. S. Kimball, Y. Yi, S. Running, K. Guan, K. Jensco, B. Maxwell, and M. Maneta, 2019: Impacts of the 2017 flash drought in the US Northern Plains informed by satellite-based evapotranspiration and solar-induced fluorescence. *Environ. Res. Lett.*, **14**, 074019, https://doi.org/10.1088/1748-9326/ab22c3.

Hoell, A., and Coauthors, 2020: Lessons learned from the 2017 flash drought across the U.S. northern Great Plains and Canadian Prairies. *Bull. Amer. Meteor. Soc.*, **101**, E2171–E2185, https://doi.org/10.1175/BAMS-D-19-0272.1.

Hunt, E., and Coauthors, 2021: Agricultural and food security impacts from the 2010 Russia flash drought. *Wea. Climate Extremes*, **34**, 100383, https://doi.org/10.1016/j.wace.2021.100383.

Hunt, E. D., K. G. Hubbard, D. A. Wilhite, T. J. Arkebauer, and A. L. Dutcher, 2009: The development and evaluation of a soil moisture index. *Int. J. Climatol.*, **29**, 747–759, https://doi.org/10.1002/joc.1749.

——, M. Svoboda, B. Wardlow, K. Hubbard, M. Hayes, and T. Arkebauer, 2014: Monitoring the effects of rapid onset of drought on non-irrigated maize with agronomic data and climate-based drought indices. *Agric. For. Meteor.*, **191**, 1–11, https://doi.org/10.1016/j.agrformet.2014.02.001.

Jolly, W. M., R. Nemani, and S. W. Running, 2005: A generalized, bioclimatic index to predict foliar phenology in response to climate. *Global Change Biol.*, **11**, 619–632, https://doi.org/10.1111/j.1365-2486.2005.00930.x.

Kimm, H., K. Guan, P. Gentine, J. Wu, C. J. Bernacchi, B. N. Sulman, T. J. Griffis, and C. Lin, 2020: Redefining droughts for the U.S. Corn Belt: The dominant role of atmospheric vapor pressure deficit over soil moisture in regulating stomatal behavior of Maize and Soybean. *Agric. For. Meteor.*, **287**, 107930, https://doi.org/10.1016/j.agrformet.2020.107930.

Koster, R. D., and Coauthors, 2004: Regions of strong coupling between soil moisture and precipitation. *Science*, **305**, 1138–1140, https://doi.org/10.1126/science.1100217.

Lai, C.-T., and G. Katul, 2000: The dynamic role of root-water uptake in coupling potential to actual transpiration. *Adv. Water Resour.*, **23**, 427–439, https://doi.org/10.1016/S0309-1708(99)00023-8.

Lisonbee, J., M. Woloszyn, and M. Skumanich, 2021: Making sense of flash drought: Definitions, indicators, and where we go from here. *J. Appl. Serv. Climatol.*, **2021** (1), 1–19, https://doi.org/10.46275/JOASC.2021.02.001.

Liu, L., L. Gudmundsson, M. Hauser, D. Qin, S. Li, and S. I. Seneviratne, 2020: Soil moisture dominates dryness stress on ecosystem production globally. *Nat. Commun.*, **11**, 4892, https://doi.org/10.1038/s41467-020-18631-1.

Lobell, D. B., M. J. Roberts, W. Schlenker, N. Braun, B. B. Little, R. M. Rejesus, and G. L. Hammer, 2014: Greater sensitivity to drought accompanies maize yield increase in the US Midwest. *Science*, **344**, 516–519, https://doi.org/10.1126/science.1251423.

Lowman, L., and A. P. Barros, 2016: Predicting phenologic response to water stress and implications for carbon uptake across the Southeast US. *2016 Fall Meeting*, San Francisco, CA, Amer. Geophys. Union, Abstract B33E-0653.

Lowman, L. E. L., and A. P. Barros, 2018: Predicting canopy biophysical properties and sensitivity of plant carbon uptake to water limitations with a coupled eco-hydrological framework. *Ecol. Modell.*, **372**, 33–52, https://doi.org/10.1016/j.ecolmodel.2018.01.011.

Luo, L., and Y. Zhang, 2012: Did we see the 2011 summer heat wave coming? *Geophys. Res. Lett.*, **39**, L09708, https://doi.org/10.1029/2012GL051383.

McEvoy, D. J., J. L. Huntington, M. T. Hobbins, A. Wood, C. Morton, M. Anderson, and C. Hain, 2016: The Evaporative Demand Drought Index. Part II: CONUS-wide assessment against common drought indicators. *J. Hydrometeor.*, **17**, 1763–1779, https://doi.org/10.1175/JHM-D-15-0122.1.

Medrano, H., J. M. Escalona, J. Bota, J. Gulías, and J. Flexas, 2002: Regulation of photosynthesis of C3 plants in response to progressive drought: Stomatal conductance as a reference parameter. *Ann. Bot.*, **89**, 895–905, https://doi.org/10.1093/aob/mcf079.

Miller, D. A., and R. A. White, 1998: A conterminous United States multilayer soil characteristics dataset for regional climate and hydrology modeling. *Earth Interact.*, **2**, https://doi.org/10.1175/1087-3562(1998)002<0001:ACUSMS>2.3.CO;2.

Mo, K. C., and D. P. Lettenmaier, 2015: Heat wave flash droughts in decline. *Geophys. Res. Lett.*, **42**, 2823–2829, https://doi.org/10.1002/2015GL064018.

Monteith, J., and M. Unsworth, 2013: *Principles of Environmental Physics: Plants, Animals, and the Atmosphere*. Academic Press, 422 pp.

Moradkhani, H., S. Sorooshian, H. V. Gupta, and P. R. Houser, 2005: Dual state–parameter estimation of hydrological models using ensemble Kalman filter. *Adv. Water Resour.*, **28**, 135–147, https://doi.org/10.1016/j.advwatres.2004.09.002.

Myneni, R., Y. Knyazikhin, and T. Park, 2015: MOD15A2H MODIS/Terra Leaf Area Index/FPAR 8-Day L4 global 500 m SIN grid V006. NASA EOSDIS Land Processes DAAC, accessed 21 July 2021, https://lpdaac.usgs.gov/products/mod15a2hv006/.

Novick, K. A., and Coauthors, 2016: The increasing importance of atmospheric demand for ecosystem water and carbon fluxes. *Nat. Climate Change*, **6**, 1023–1027, https://doi.org/10.1038/nclimate3114.

Oren, R., J. S. Sperry, G. G. Katul, D. E. Pataki, B. E. Ewers, N. Phillips, and K. V. R. Schäfer, 1999: Survey and synthesis of intra- and interspecific variation in stomatal sensitivity to vapour pressure deficit. *Plant Cell Environ.*, **22**, 1515–1526, https://doi.org/10.1046/j.1365-3040.1999.00513.x.

Osman, M., B. F. Zaitchik, H. S. Badr, J. I. Christian, T. Tadesse, J. A. Otkin, and M. C. Anderson, 2021: Flash drought onset over the contiguous United States: Sensitivity of inventories and trends to quantitative definitions. *Hydrol. Earth Syst. Sci.*, **25**, 565–581, https://doi.org/10.5194/hess-25-565-2021.

Otkin, J. A., M. C. Anderson, C. Hain, I. E. Mladenova, J. B. Basara, and M. Svoboda, 2013: Examining rapid onset drought development using the thermal infrared–based Evaporative Stress Index. *J. Hydrometeor.*, **14**, 1057–1074, https://doi.org/10.1175/JHM-D-12-0144.1.

——, ——, ——, and M. Svoboda, 2014: Examining the relationship between drought development and rapid changes in the Evaporative Stress Index. *J. Hydrometeor.*, **15**, 938–956, https://doi.org/10.1175/JHM-D-13-0110.1.

——, and Coauthors, 2016: Assessing the evolution of soil moisture and vegetation conditions during the 2012 United States flash drought. *Agric. For. Meteor.*, **218–219**, 230–242, https://doi.org/10.1016/j.agrformet.2015.12.065.

——, M. Svoboda, E. D. Hunt, T. W. Ford, M. C. Anderson, C. Hain, and J. B. Basara, 2018: Flash droughts: A review and assessment of the challenges imposed by rapid-onset droughts in the United States. *Bull. Amer. Meteor. Soc.*, **99**, 911–919, https://doi.org/10.1175/BAMS-D-17-0149.1.

——, Y. Zhong, E. D. Hunt, J. Basara, M. Svoboda, M. C. Anderson, and C. Hain, 2019: Assessing the evolution of soil moisture and vegetation conditions during a flash drought–flash recovery sequence over the south-central United States. *J. Hydrometeor.*, **20**, 549–562, https://doi.org/10.1175/JHM-D-18-0171.1.

——, and Coauthors, 2021: Development of a Flash Drought Intensity Index. *Atmosphere*, **12**, 741, https://doi.org/10.3390/atmos12060741.

Pendergrass, A. G., and Coauthors, 2020: Flash droughts present a new challenge for subseasonal-to-seasonal prediction. *Nat. Climate Change*, **10**, 191–199, https://doi.org/10.1038/s41558-020-0709-0.

Rawls, W. J., and D. L. Brakensiek, 1982: Estimating soil water retention from soil properties. *J. Irrig. Drain. Div.*, **108**, 166–171, https://doi.org/10.1061/JRCEA4.0001383.

——, T. J. Gish, and D. L. Brakensiek, 1991: Estimating soil water retention from soil physical properties and characteristics. *Advances in Soil Science*. B. A. Stewart, Ed., Advances in Soil Science, Vol. 16, Springer, 213–234, https://doi.org/10.1007/978-1-4612-3144-8_5.

——, L. R. Ahuja, D. L. Brakensiek, and A. Shirmohammadi, 1992: Infiltration and soil water movement. *Handbook of Hydrology*, D. R. Maidment, Ed., McGraw-Hill Inc., 5–51.

Rigden, A. J., N. D. Mueller, N. M. Holbrook, N. Pillai, and P. Huybers, 2020: Combined influence of soil moisture and atmospheric evaporative demand is important for accurately predicting US maize yields. *Nat. Food*, **1**, 127–133, https://doi.org/10.1038/s43016-020-0028-7.

Rippey, B. R., 2015: The U.S. drought of 2012. *Wea. Climate Extremes*, **10**, 57–64, https://doi.org/10.1016/j.wace.2015.10.004.

Savitzky, A., and M. J. E. Golay, 1964: Smoothing and differentiation of data by simplified least squares procedures. *Anal. Chem.*, **36**, 1627–1639, https://doi.org/10.1021/ac60214a047.

Sellers, P. J., C. J. Tucker, G. J. Collatz, S. O. Los, C. O. Justice, D. A. Dazlich, and D. A. Randall, 1996: A revised land surface parameterization (SiB2) for atmospheric GCMS. Part II: The generation of global fields of terrestrial biophysical parameters from satellite data. *J. Climate*, **9**, 706–737, https://doi.org/10.1175/1520-0442(1996)009<0706:ARLSPF>2.0.CO;2.

Smith, A. B., 2020: U.S. billion-dollar weather and climate disasters, 1980–present (NCEI Accession 0209268). NOAA National Centers for Environmental Information, https://www.ncei.noaa.gov/access/metadata/landing-page/bin/iso?id=gov.noaa.nodc:0209268.

Stöckli, R., T. Rutishauser, D. Dragoni, J. O'Keefe, P. E. Thornton, M. Jolly, L. Lu, and A. S. Denning, 2008: Remote sensing data assimilation for a prognostic phenology model. *J. Geophys. Res.*, **113**, G04021, https://doi.org/10.1029/2008JG000781.

Sulman, B. N., D. T. Roman, K. Yi, L. Wang, R. P. Phillips, and K. A. Novick, 2016: High atmospheric demand for water can limit forest carbon uptake and transpiration as severely as dry soil. *Geophys. Res. Lett.*, **43**, 9686–9695, https://doi.org/10.1002/2016GL069416.

Svoboda, M., and Coauthors, 2002: The Drought Monitor. *Bull. Amer. Meteor. Soc.*, **83**, 1181–1190, https://doi.org/10.1175/1520-0477-83.8.1181.

Tobin, K. J., W. T. Crow, J. Dong, and M. E. Bennett, 2019: Validation of a new root-zone soil moisture product: Soil merge. *IEEE J. Sel. Top. Appl. Earth Obs. Remote Sens.*, **12**, 3351–3365, https://doi.org/10.1109/JSTARS.2019.2930946.

Vicente-Serrano, S. M., S. Beguería, and J. I. López-Moreno, 2010: A multiscalar drought index sensitive to global warming: The standardized precipitation evapotranspiration index. *J. Climate*, **23**, 1696–1718, https://doi.org/10.1175/2009JCLI2909.1.

Wang, H., S. D. Schubert, R. D. Koster, and Y. Chang, 2019: Attribution of the 2017 northern High Plains drought [in "Explaining Extreme Events of 2017 from a Climate

Perspective"]. *Bull. Amer. Meteor. Soc.*, **100** (1), S25–S29, https://doi.org/10.1175/BAMS-D-18-0115.1.

Wilhite, D. A., and M. H. Glantz, 1985: Understanding: The drought phenomenon: The role of definitions. *Water Int.*, **10**, 111–120, https://doi.org/10.1080/02508068508686328.

Williams, A. P., B. I. Cook, J. E. Smerdon, D. A. Bishop, R. Seager, and J. S. Mankin, 2017: The 2016 southeastern U.S. drought: An extreme departure from centennial wetting and cooling. *J. Geophys. Res. Atmos.*, **122**, 10 888–10 905, https://doi.org/10.1002/2017JD027523.

——, and Coauthors, 2020: Large contribution from anthropogenic warming to an emerging North American megadrought. *Science*, **368**, 314–318, https://doi.org/10.1126/science.aaz9600.

Xia, Y., and Coauthors, 2012: Continental-scale water and energy flux analysis and validation for the North American Land Data Assimilation System project phase 2 (NLDAS-2): 1. Intercomparison and application of model products. *J. Geophys. Res.*, **117**, D03109, https://doi.org/10.1029/2011JD016048.

Zhang, M., and X. Yuan, 2020: Rapid reduction in ecosystem productivity caused by flash droughts based on decade-long FLUXNET observations. *Hydrol. Earth Syst. Sci.*, **24**, 5579–5593, https://doi.org/10.5194/hess-24-5579-2020.

Zhou, S., R. A. Duursma, B. E. Medlyn, J. W. G. Kelly, and I. C. Prentice, 2013: How should we model plant responses to drought? An analysis of stomatal and non-stomatal responses to water stress. *Agric. For. Meteor.*, **182–183**, 204–214, https://doi.org/10.1016/j.agrformet.2013.05.009.

——, and Coauthors, 2019: Land–atmosphere feedbacks exacerbate concurrent soil drought and atmospheric aridity. *Proc. Natl. Acad. Sci. USA*, **116**, 18 848–18 853, https://doi.org/10.1073/pnas.1904955116.